

Guiding, Modulating, and Emitting Light on Silicon—Challenges and Opportunities

Michal Lipson, *Member, IEEE*

Invited Paper

Abstract—Silicon photonics could enable a chip-scale platform for monolithic integration of optics and microelectronics for applications of optical interconnects in which high data streams are required in a small footprint. This paper discusses mechanisms in silicon photonics for waveguiding, modulating, light amplification, and emission. These mechanisms, together with recent advances of fabrication techniques, have enabled the demonstration of ultracompact passive and active silicon photonic components with very low loss.

Index Terms—Integrated optics, light emitters, modulators, silicon, waveguides.

I. INTRODUCTION

THERE have been several advances in the field of integrated photonics in the last few years, with most of them directed towards the telecommunication industry at 1.5 μm . Devices including filters, modulators, and routers are fabricated using a variety of materials like LiNbO_3 , GaAs, and InP. These specific materials are used due to their excellent electrooptic properties and emissive capabilities. For pure telecommunication applications, where the optical components are usually discrete, these materials are excellent candidates.

Recently, there have been alternative emerging applications for photonics, where the demand for greater bandwidth requires the advantages provided by optics for interconnections [1]–[5]. The most likely insertion points for integrated photonics into systems will be in places where an extreme amount of data is required to travel in a very small space [6]. Two examples of applications are for microprocessor data buses (i.e., from microprocessor to memory or between multiple processors) and in the backplane of server racks. These applications involve an increase in complexity in the optical domain that requires

greater integration of optical and electronic components. Monolithic integration of a suite of optical and electronic capabilities on one substrate is the natural progression for the vision of an integrated photonic system.

Using Si for optical interconnects would enable a platform for such a monolithic integration of optics and microelectronics [6]–[9]. Photonics on silicon has been suggested since the 1980s [10]. It is only in the last few years, however, that submicrometer-size photonic structures have been realized [7]. The challenges of using silicon as a photonic material are the high propagation losses (due to scattering off the waveguide's sidewalls), low electrooptic coefficient, low light-emission efficiency, and high fiber-to-waveguide coupling losses. The recent progress of nanofabrication techniques, however, enabled the demonstration of a large number of ultracompact high-performance photonic components, overcoming the traditional limitations of silicon photonics.

Low-loss waveguides with propagation losses less than 3 dB/cm have been demonstrated recently [11], [12]. These waveguides with submicrometer-size cross-sectional dimensions are strong light confining, with most of the field concentrated at its core. Tapers for fiber–waveguide coupling with very low coupling losses have been demonstrated as well [13], [14]. These tapers enable the conversion of modes with cross-sectional dimensions of several of micrometers down to only a few hundreds of nanometers, in a very small length. There have recently been several demonstrations of highly compact wavelength-division-multiplexing (WDM) silicon devices for on-chip high-bandwidth applications. These devices with channel spacing down to 0.1 nm [15]–[17] were achieved using a variety of geometrical configurations. In the last few years, efforts in silicon photonics have been directed more towards active photonic devices such as modulators, amplifiers, and light emitters. High-speed electrooptic modulators with speeds up to 10 Gb/s [18], [19] have been demonstrated in silicon using different geometries, with sizes down to only a few micrometers [20]. There have also been several efforts in the last two decades on obtaining light emission and gain out of silicon using materials ranging from bulk silicon to Er:Si [21]. The objective of these investigations is to induce emission through carriers injected in the silicon, enabling therefore, electrooptic silicon lasers. Recently, gain of 12 cm^{-1} has been obtained in silicon nanocrystals (Si-nc) [22] using carrier-confinement effects. In order to obtain amplification in silicon waveguides

Manuscript received August 31, 2004; revised June 3, 2005. This work was supported by the National Science Foundation (NSF) under Contract ECS-0300387 and CAREER Grant 0446571; the Cornell Center for Nanoscale Systems; the National Science Foundation (NSF), Semiconductor Research Corporation under Grant 2005-RJ-1296; the Air Force Office of Scientific Research (AFOSR) under Grant AFOSR F49620-03-1-0424 and FA9550-05-C-0102; and the Science and Technology Centers (STC) program of the NSF under agreement DMR-0120967. This work has been partially carried out as part of the Interconnect Focus Center Research Program at Cornell University, supported in part by the Microelectronics Advanced Research Corporation (MARCO), its participating companies, and DARPA.

The author is with the School of Electrical and Computer Engineering, Cornell University, Ithaca, NY 14853-0001 USA (e-mail: lipson@ece.cornell.edu; m1292@cornell.edu).

Digital Object Identifier 10.1109/JLT.2005.858225

using optical pumping (as opposed to electrooptical pumping) Raman scattering can be used. In [23]–[26], gain in the range of 2–11 dB has been reported in centimeter-sized silicon waveguides. Using Raman amplification, an all-optically pumped silicon laser with a linewidth of less than 80 MHz was demonstrated in [20] using a compact waveguide cavity.

The advancement of the field of silicon photonics relies on further investigation of individual enabling devices as well as on the development of integrated systems based on such devices. Although propagation losses of waveguides have been significantly reduced in the last few years, the further reduction of the losses below 1 dB/cm in highly confining waveguides, requires a carefully study of the surfaces involved; it is not clear whether the measured losses are induced by surface scattering or by some additional absorption mechanism. The demonstration of a silicon laser remains a high-profile research topic in the scientific community, despite the fact that a silicon laser may not be a bottleneck for the implementation of silicon photonics. WDM offers the ability for on-chip data transmission with extremely high bandwidth. Passive WDM devices as well as active silicon modulators have been demonstrated, however, the use of WDM devices for the demonstration of high bandwidth on a silicon chip remains to be demonstrated. The robustness of the demonstrated enabling devices to changes in environmental conditions such as temperature needs to be demonstrated. This is especially true for devices relying on resonant effects, which are highly sensitive to small changes in the index of refraction. Packaging of the integrated devices, especially incoming and outgoing ports to and from fibers for enabling inexpensive fast assembly remains a challenge. The demonstration of integrated systems on a chip with new architectures that are based on silicon photonics, for applications requiring high bandwidth and low power, ranging from optical interconnects to sensing, is needed. The development of such systems requires the investigation of issues related to the integration of different devices such as waveguides, amplifiers, and modulators. Finally, the integration of silicon with electronics requires the development of a process that allows for thermal isolation between the electronic and photonic elements, optical isolation, and the integration of photosensitive layers and high-quality optically transparent layers.

This paper is divided into three sections. Section II describes light propagation in Si waveguides. Different types of silicon waveguides are described in Section II-A. The origin of propagation losses due to radiation and light scattering are described in Sections II-B and C. Recent works demonstrating extremely low-loss passive silicon devices are discussed in Section II-D. Section III describes active Si photonic devices such as switches and modulators. Several successful geometrical configurations and physical mechanisms for externally modifying the optical properties of integrated devices are described in Sections III-A and B. Section IV discusses physical mechanisms that are being explored to develop a silicon light emitter, as well as current efforts for coupling external light sources to the chip. A silicon emitter is the missing piece for complete monolithic integration. Until a reliable and efficient silicon emitter can be produced, hybrid integration must be considered: using a nonsilicon-based light source from a fiber

coupled to silicon waveguides. In Section IV-A, we describe schemes for coupling external fibers to submicrometer-size waveguides that enable this hybrid approach. While a silicon laser is still out of reach, research is being done worldwide on silicon light emitters. In Section IV-B, we describe schemes for achieving gain and lasing in silicon. The current efforts in detection in the field of Si photonics, in the near-infrared wavelength range, are mainly geared towards the integration of SiGe alloys on silicon substrates, with Ge-concentrations exceeding 50%. Due to the 4% lattice mismatch between Si and Ge, the growth of SiGe layers on Si substrates is restricted to a critical thickness, above which threading dislocations degrade the material, affecting the dark current, and hence, the noise factor. Current efforts in the development of photodetectors on silicon in the near-infrared spectral region are mainly directed towards growth techniques and schemes for material integration [28]–[30]. These efforts are not discussed in this paper, which is focused on the development of components based on silicon material.

II. LIGHT PROPAGATION IN Si WAVEGUIDES

Propagation losses in integrated optical structures originate from three main different sources: coupling to radiation modes, intrinsic absorption in the material, and scattering due to imperfections in the fabrication of the waveguide. Here, we focus on waveguides operating at the wavelength of telecommunication in the spectral range around 1.55 μm . In this wavelength range, losses due to intrinsic absorption in both Si and SiO₂ can be neglected [31] when compared to the losses due to radiation modes and to light scattering. Below, we describe typical waveguides used in silicon photonics, coupling to radiation modes and scattering processes in silicon waveguides, and several novel geometries and fabrication processes developed for overcoming losses. We also describe several passive silicon waveguiding devices with high performance that were recently demonstrated.

A. Types of Waveguides

Several types of waveguides with different geometries and light-guiding mechanisms can be used in silicon. In general, the geometry of the waveguide depends on the device in which the waveguide is incorporated. Waveguides with large cross-sectional dimensions are usually integrated in devices requiring propagation over relatively short straight paths with no bends while waveguides with smaller cross-sectional dimensions are used in devices requiring long lengths. As discussed in the subsequent section, waveguides with large cross-sectional dimensions are usually easier to couple to the input and output of a typical 10- μm core fiber. They require a large bending radius, however, and therefore, devices based on waveguides are usually discrete since on-chip integration is difficult. Waveguides with smaller cross-sectional dimensions suffer from high coupling losses due to the difference in size between the mode of a fiber and that of a waveguide. Their small dimensions, however, enable ultracompact devices to be integrated on-chip. Also, as we describe below, their high-confinement nature offer the ability to enhance light in small regions, enabling novel active

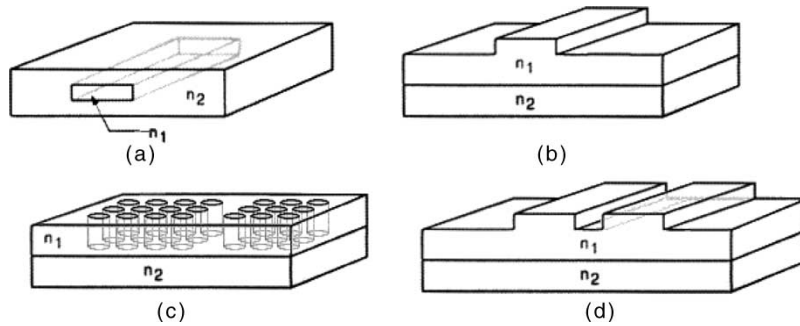


Fig. 1. Four configurations of waveguides in silicon. (a) Channel waveguides. (b) Ridge waveguides. (c) Photonic-crystal waveguides. (d) Slot waveguides.

devices like modulators and amplifiers by effectively enhancing the optical properties of silicon in these regions.

The most standard waveguides used for silicon photonics are channel waveguides and ridge waveguides [see Fig. 1(a) and (b)]. In channel waveguides, the guiding layer is completely surrounded by a cladding layer, while in ridge waveguides, the guiding layer consists of a slab with a dielectric ridge on top embedded between two low-index-of-refraction layers (the top layer can also be left uncladded). The dielectric ridge creates an effective-high-index region just below the ridge, with a slightly higher effective index than the index of the slab. In both the channel and the ridge waveguides, light is confined due to total internal reflection between the high- and low-index-of-refraction region. The typical cross-sectional dimensions of these two waveguide configurations are determined by the effective refractive index n_{eff} in the guiding region, which determines the degree of light confinement in the core. Channel waveguides typically have submicrometer cross-sectional dimensions due to their larger effective index ($n_{\text{eff}} \sim 3$). Ridge waveguides, in contrast, enable relatively large optical modes, on the order of a few micrometers, to be confined in silicon without sacrificing single-mode operation [32], [33], despite the fact that the high index contrast between silicon (core) and oxide or air (cladding) seems to imply a small mode size. This is due to the ridge-waveguide geometry that induces a relatively low effective index ($n_{\text{eff}} \sim 2$).

The channel and ridge waveguides described above are based on the principle of total internal reflection, where light is concentrated in the high-index-of-refraction region of the waveguide. In addition to these waveguides, a silicon platform, due to its especially high index of refraction (in contrast to glass materials, for example), enables other novel types of waveguides where light can be confined in low indices of refraction regions (as air). These are photonic crystal waveguides [Fig. 1(c)] and slot waveguides [Fig. 1(d)].

Photonic crystals [34] are periodic dielectric structures composed of alternating regions of dielectric materials with high and low index of refraction, with periodicity on the order of the wavelength of light. This periodicity induces a very high reflectivity in a spectral range for which light cannot propagate in the crystal, equivalent to the energy gap formed in a semiconductor crystal. If the photonic crystal is formed by dielectric materials with high index contrast $n_H - n_L > 1.5$, where n_H and n_L are the high and low indices, this reflectivity can occur for all directions of light incident on the crystal, and the crystal is said

to have a complete photonic bandgap. Silicon offers an ideal platform for creating photonic crystals with complete band gaps due to its high index of refraction. The periodicity of the photonic crystal can be in one, two, or three dimensions. One-dimensional (1-D) photonic crystals can be created by simple deposition techniques of multilayers (as sputtering or chemical-vapor deposition). Two-dimensional (2-D) photonic crystals can be created using conventional lithographic processes developed originally for the semiconductor-electronic industry. The fabrication of three-dimensional (3-D) photonic crystals still remains a challenge [35]. Optical waveguides based on photonic crystals can be created by surrounding channel waveguides with a photonic-crystal region. Light constructively interferes in the channel-waveguiding region and destructively interferes in the photonic-crystal region. These optical waveguides are usually formed by removing materials from a 2-D photonic crystal, for creating channels in the crystal through which light can propagate. In the plane of the crystal, light is confined in the channel waveguide due to the photonic-crystal effect. Out of the plane of the crystal, light is confined due to total internal reflection, since the effective index in the channel is larger than the effective index in the top and bottom cladding layers. In order to ensure that total internal reflection indeed takes place, silicon photonic crystals are often formed using air as top and bottom cladding by fabricating air-bridge structures [35]. Due to their waveguiding mechanism, photonic-crystal waveguides can guide light in cores with cross-sectional dimensions smaller than $0.15 \mu\text{m}$.

We have suggested recently a new type of waveguide [37], a “slot waveguide” that can confine light in low-index-of-refraction regions (Fig. 2). The structure is based on a low index submicrometer slot (air or SiO_2) embedded between two silicon waveguides. Due to the high index contrast, modes with strong field intensity at the two interfaces of the slot are formed. The overlap of the evanescent tail of the modes in the central slot leads to a strong light confinement in the low-index region. The net effect is a stronger field intensity in the slot relative to the one in the silicon region. We show experimentally in [38] that, using these structures, light can be confined in low-index regions that can be as small as 50 nm in width. Note that in contrast to the photonic-crystal waveguides described above, the high-confinement modes in the slot region are true eigenmodes and are therefore theoretically lossless (assuming that there are no scattering points along the structures). Fig. 2(a) shows the cross-sectional field distribution in an Si/SiO_2 slot waveguide. The fabricated structure is shown in Fig. 2(b).

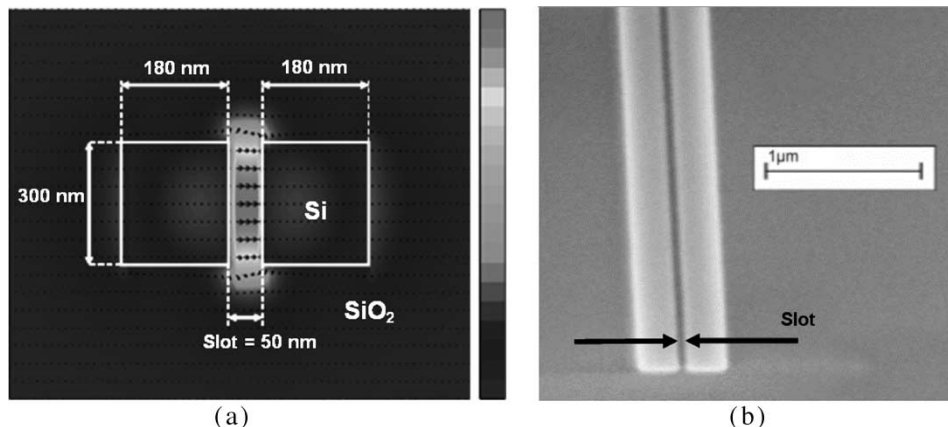


Fig. 2. (a) Cross-sectional field distribution in a Si/SiO₂ slot waveguide. (b) SEM of the fabricated slot-waveguide structure (top view).

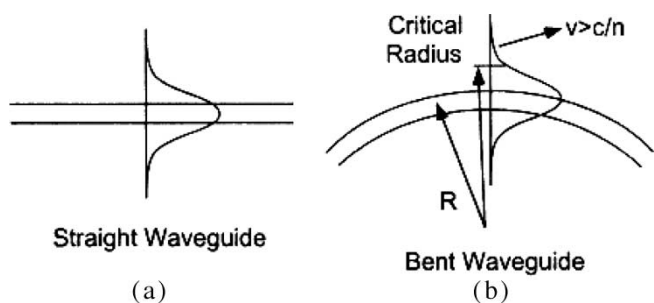


Fig. 3. (a) Mode-field distribution in a straight waveguide. (b) Mode-field distribution in a bent waveguide.

B. Losses Due to Coupling to Radiation Modes

Coupling of guiding modes to radiation modes is an important loss factor in silicon waveguides. For a single-mode waveguide, it occurs when the geometry of the waveguide is strongly altered, as in bended waveguides. Silicon photonics relies on tight bending radii for dense integration on-chip; it is therefore important to avoid losses due to radiation.

In order to understand the mechanism of coupling to radiation modes in bends, consider Fig. 3(a), showing the mode-field distribution in a straight waveguide [39], [40]. If the waveguide is bent [Fig. 3(b)], the spatial mode is not appreciably changed in shape compared to the straight waveguide. The wavefronts associated with the mode, however, are now pivoted about the center of curvature of the bend. To keep up with the propagating mode in the waveguide, the phase front on the outside of the bend in the cladding region must travel slightly faster than the phase front in the core. At some critical distance from the core of the waveguide, the phase front will have to travel faster than the local speed of light c/n , where n is the index of the cladding. Since this is not possible, the field beyond this critical radius breaks away and enters a radiating mode. The light that leaks away from the waveguide is therefore a loss in power.

Single-mode waveguides are used in order to minimize radiation losses on-chip. This is because when light is distributed across the chip using bends, the higher order modes, which are less confined in the waveguides, tend to leak out of the waveguides. For single-mode waveguides, the smallest radius for which radiation losses are minimal is smaller for a higher degree of light confinement in the waveguide. In a high-

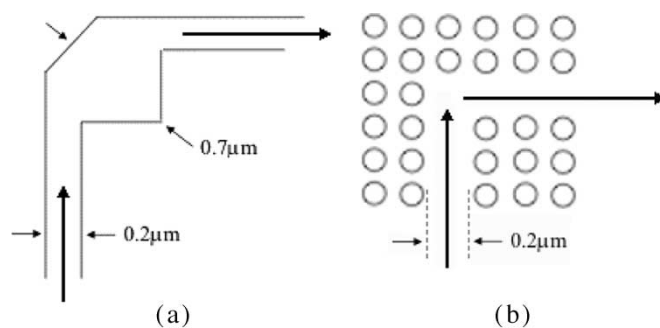


Fig. 4. Schematics of the top view of a sharp 90° bend in (a) a modified channel waveguide and (b) a 2-D photonic-crystal waveguide.

confinement waveguide, the mode is mostly contained in the waveguide core and is only slightly affected by a tight bending of the waveguide, while in a low-confinement waveguide, there is a large field distribution outside the core of the waveguide and radiation easily occurs when the waveguide is bent. In standard waveguides relying on total internal reflection, the degree of confinement is proportional to the effective-index-of-refraction contrast of the waveguide. For example, for Si/SiO₂ channel waveguides, where the degree of confinement is high, the minimum bending radius is a few micrometers, while for ridge waveguides, where the degree of confinement is low, the bending radius is required to be as large as a few hundred micrometers.

In order to further shrink the bending radius of a silicon waveguide and enable a high density of photonic devices on-chip, modified channel waveguides can be used to create 90° bends. In these structures, the bend is modified to ensure that the mode is pulled inside the bend, preventing light from leaking from the waveguide. For example, in the structure shown in Fig. 4(a), additional material is added to the inner part of the bend and is removed from the outer part of the bend. The net effect is a higher effective index in the internal part of the bend. This induces a modification of the mode distribution in the bend region, with a smaller overlap with the outer part of the bend, preventing it from radiating out of the waveguide. Using these structures, the authors in [41] have shown a 90° bend with submicrometer dimensions and losses of less than 1% per bend.

Photonic crystals also enable light guiding in extremely sharp bends [42]. Light which travels in channels surrounded by

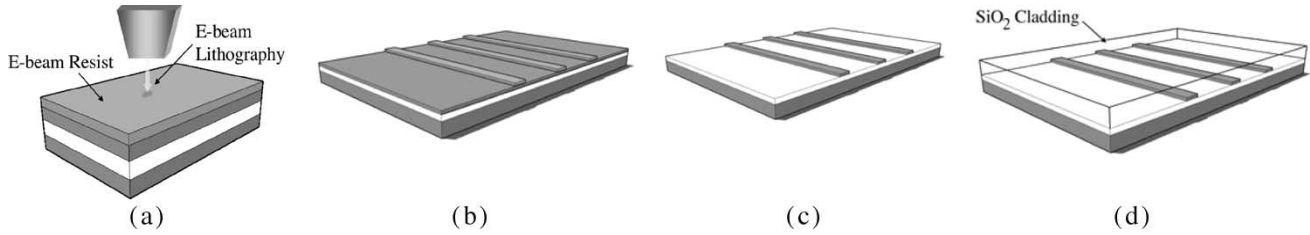


Fig. 5. Fabrication process of channel silicon waveguides. (a) Negative electron-beam resist is spun on the SOI wafer. Photonic structures are defined by electron-beam lithography. (b) The resist is developed leaving the resist mask. (c) RIE is used to etch the pattern into the top silicon layer, down to the BOX layer. (d) The device is covered with a cladding of oxide.

photonic crystals is completely reflected by the surrounding region of space, enabling light to be guided in unconventional ways [see Fig. 4(b)]. In fact, the low losses in bent waveguides have been one of the main motivations for the development of photonic crystals on silicon. Photonic-crystal waveguides with a bending radius of less than 1 μm and low losses have successfully been demonstrated [42].

C. Losses Due to Scattering

The main source of losses in silicon single-mode waveguides is the scattering off the roughness of the sidewalls. As previously discussed, the waveguides that are desired for high-density silicon photonics are those with extremely small cross-sectional dimensions, allowing them to have small bending radii. The imperfections in fabrication are significant in size compared to the dimensions of these waveguides, resulting in high losses. For example, losses in channel waveguides typically range from 0.2 to 5 dB/cm [11]. Losses in photonic-crystal and slot waveguides are even higher. In contrast, rib waveguides, due to their larger dimensions, have typically lower losses of less than 0.1 dB/cm [43].

The scattering losses are highly dependent on the fabrication process of waveguides. In order to understand the origin of these losses, we describe in Fig. 5, a typical fabrication process for channel waveguides on a silicon-on-insulator (SOI) platform. The process begins with an SOI wafer. A negative electron-beam resist, a material that becomes insoluble in developing solutions when exposed to radiation, is spun on the wafer [see Fig. 5(a)]. Photonic structures are then defined by electron-beam lithography. The resist is then developed leaving the resist mask [see Fig. 5(b)]. The pattern is etched into the top silicon layer, down to the buried oxide (BOX) layer, using reactive ion etching (RIE) [see Fig. 5(c)]. Finally, the device is covered with a cladding of oxide using, for example, plasma-enhanced chemical-vapor deposition (PECVD). Note that although the small feature sizes of the waveguides fabricated in this process rely on e-beam lithography, these lithography steps can also be achieved using extreme UV lithography.

The deposition process results in an even and uniform film, thus providing a very smooth surface for the top and bottom of the waveguide. However, the sidewalls of the waveguide have significant roughness, since these are formed by a dry-etching process through the mask. The dynamics of the etching and the imperfections in the mask lead to small bumps and ridges (aberrations) on the sidewall of the waveguides.

Physically, the effect of small perturbations on the waveguide walls can be viewed as being identical to the small random density fluctuations in glass that lead to Rayleigh scattering in fibers. The propagation losses α are proportional to the index contrast between the core and the cladding Δn , the size of the roughness σ , and the normalized field intensity at the core/cladding interface [44].

$$\alpha = \frac{\sigma^2 k_0^2 n_{\text{core}}}{n_{\text{eff}}} \cdot \frac{E_S^2}{\int E^2 dx} \cdot \Delta n^2 \quad (1)$$

where k_0 is the free-space wavenumber, E_S is the field intensity at the core/cladding interface, E is the field intensity at a position x along the cross section of the waveguide, and n_{eff} is the effective index of refraction. In silicon waveguides, Δn is relatively large (~ 2), inducing high propagation losses.

When the sidewall roughness is periodic along the waveguide, the losses are affected not only by the amplitude of the roughness, but also by the autocorrelation length, i.e., the mean distance between the scattering points. When the autocorrelation length is comparable to the wavelength, the waveguide with regular scattering points acts as a grating and losses increase. If the autocorrelation length approaches one quarter of the wavelength in the material (~ 150 nm), the scattering losses can be very large: for $\sigma = 5$ nm, the losses in a single-mode channel waveguide are approximately 10 dB/cm.

Losses due to scattering can be reduced using geometries that minimize the mode overlap with the rough sidewalls of the waveguide, $E_S^2 / \int E^2 dx$ in (1). Fig. 6 shows a numerically simulated mode in two possible rectangular channel-waveguide configurations. The high intensity of the mode is represented by dark gray, while the low intensity is represented by light gray. The waveguide in Fig. 6 is assumed to be fabricated on a wafer oriented along the X direction. The sidewalls of the waveguides along the Y direction, defined using photolithography, have bumps and ridges. In Fig. 6(a), the horizontal geometry ensures that the mode overlap with the rough sidewalls is minimal. Losses in a waveguide with this orientation are expected to be low. Fig. 6(b) shows a vertical-geometry waveguide in which the mode overlap with the rough sidewalls is high. In a waveguide with a high aspect ratio, losses are expected to be high.

The scattering losses induce a wavelength dependence of the transmission efficiency [12]. This is a result of two competing wavelength-dependent processes. First, there exists a dependence of the modal distribution on wavelength. For a waveguide designed to operate in single mode at 1500 nm,

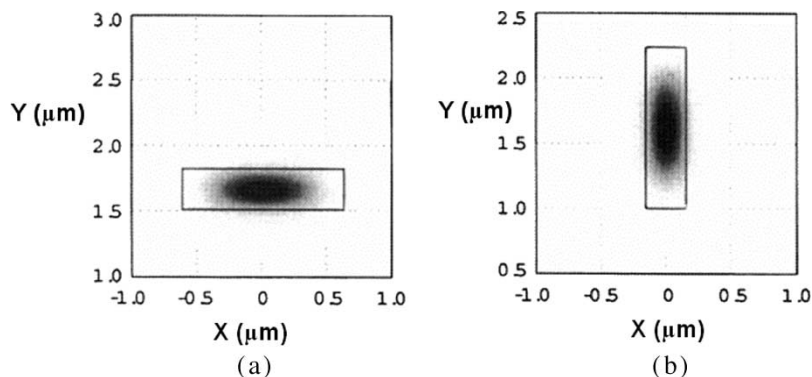


Fig. 6. (a) Channel waveguide in horizontal geometry where the mode overlap with the rough sidewalls has been minimized. (b) Channel waveguide in vertical geometry where the mode overlap with the rough sidewalls is high.

a higher wavelength (> 1600 nm) close to the cutoff wavelength of the waveguide will have high losses due to the increase of overlap of the field with the sidewall roughness. Second, there is a wavelength dependence of the scattering process where smaller wavelengths (< 1400 nm) have higher losses due to the increase of the roughness/wavelength ratio [see (1)]. Therefore, around 1500 nm, there is an optimum transmission window, where a relatively flat band exists.

Recently, there have been several demonstrations of submicrometer-size waveguides with low losses using high-quality fabrication processes that minimize the amplitude of the sidewall roughness. Channel silicon waveguides with losses of approximately 3.6 dB/cm with 0.2×0.4 μm cross-sectional dimensions were fabricated using e-beam lithography [11]. Another approach involves oxidizing the sidewalls of the waveguide [45], fabricated using a similar fabrication process as in [11], in order to minimize roughness. The measured propagation losses are extremely low: approximately 0.8 dB/cm.

D. Passive Devices

Using channel and ridge waveguides, several passive devices have been recently demonstrated on silicon including Mach-Zehnder-interferometer-based filters, multimode interference couplers, and wavelength-division multiplexers. Developing passive devices on a silicon platform would be a cost advantage to the telecommunication field when compared to those currently employed devices that use fibers and large oxide-based waveguides. In addition, these devices would be essential for all applications concerning on-chip silicon photonics, including high-bandwidth interconnects.

A Mach-Zehnder-interferometer-based filter uses interference between two waves to convert phase change into intensity variation. Fig. 7 shows a schematic Mach-Zehnder interferometer. The waveguide input is split into two waveguides by a Y-junction. The split beams travel different paths and then recombine at another Y-junction. If the difference between the optical path lengths of the two arms is an integer number of optical wavelengths, the two waves will arrive at the Y-junction in-phase, and constructively interfere. They will recombine into a guided mode, which then propagates down the remaining waveguide. On the other hand, if the optical path lengths differ

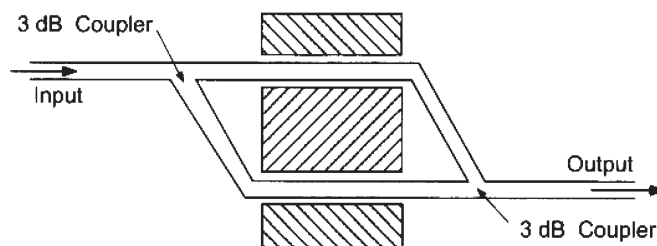


Fig. 7. Schematic of a Mach-Zehnder interferometer.

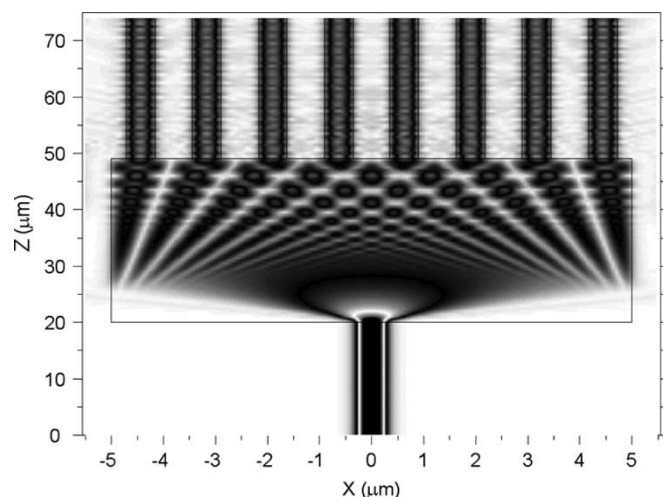


Fig. 8. Simulation of a 1×8 MMI splitter.

in phase by integer multiples of π , the two beams will destructively interfere and not couple into the following waveguide. This difference in optical-path length is wavelength dependent, and therefore the device acts as a filter. Mach-Zehnder-interferometer-based filters have been fabricated in silicon with low losses [15].

Multimode interference (MMI) couplers are $1 \times N$ splitters with a single-mode input and output waveguides separated by a slab region (see Fig. 8). The slab region supports a large number of modes that propagate with different phase velocities leading to a strong interference pattern with clear high-and-low-intensity regions. The output waveguides are placed at the positions of the high-intensity peaks. The device is able to

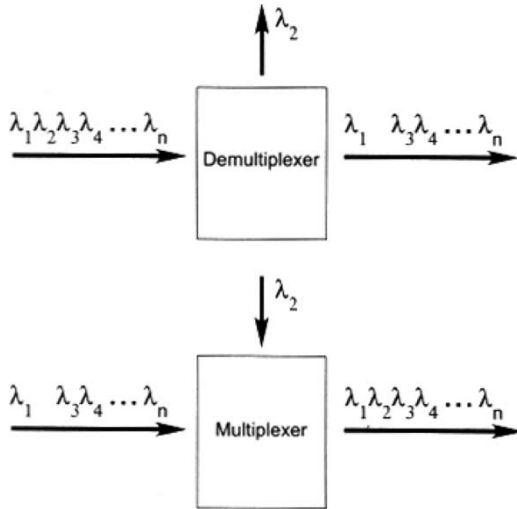


Fig. 9. Schematics of a demultiplexing and a multiplexing filter.

split a signal from a single waveguide into a large number of waveguides. It can also recombine signals coming in from a large number of waveguides into a single one. Due to the strong confinement nature of the Si/SiO₂ system, the interference pattern occurs in a smaller slab and the output waveguides can be placed close together. Hence, extremely compact couplers can be realized in this system. A 400 × 48 μm MMI coupler based on Si ridge waveguides functioning as a 1 × 8 coupler was successfully demonstrated [12]. Fig. 8 shows the intensity distribution in a 1 × 8 MMI structure based on Si/SiO₂ channel waveguides calculated using the beam-propagation method [39]. High intensity is represented by dark gray while low intensity is represented by light gray. The total size of the device is 10 × 50 μm.

Today, wavelength division multiplexing (WDM) has become a dominant device in the telecommunication field. In a WDM system, a series of discrete wavelengths are simultaneously transmitted through a waveguide bus, each one of them individually encoded. The key issue in WDM systems is finding ways to add and drop individual wavelengths from the bus while letting the remaining wavelengths travel on to their ultimate destination. Fig. 9 describes schematically the function of a multiplexing and a demultiplexing filter.

One of the most common WDM devices used in the telecommunication field is the Bragg grating (see Fig. 10) that consists of a modulated waveguide (or fiber). The reflectivity of the grating determines the selectivity filter. The higher the reflectivity, the more selective the filter is to specific wavelengths. For a period of the grating equal to $\Lambda = \lambda_0 n_L / 4 + \lambda_0 n_H / 4$, where n_L and n_H are the effective indices in the modulated regions of the grating, the reflectivity of a Bragg grating around $\lambda = \lambda_0$ can be derived considering a one-dimensional stack of materials with high-and-low effective indices, and applying the continuity of the fields at the boundaries [39]

$$R^2 = \left[\frac{\left(-\frac{n_L}{n_H}\right)^q - \left(-\frac{n_H}{n_L}\right)^q}{\left(-\frac{n_L}{n_H}\right)^q + \left(-\frac{n_H}{n_L}\right)^q} \right]^2 \quad (2)$$

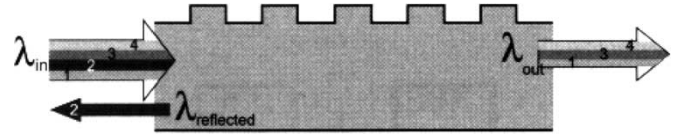


Fig. 10. Schematics of a waveguide Bragg grating.

where q is the number of periods. From (2), one can see that the higher the index contrast, the smaller the Bragg grating will be. The total length of the device is determined by the number of periods q required for high reflectivity. In low-index-contrast waveguides, the typical size of gratings is from millimeter to centimeter size. The high-index-contrast nature of the Si/SiO₂ platform enables compact Bragg gratings. In order to fabricate Bragg grating, either extreme UV photolithography or e-beam lithography is used. In [16], the authors show a high-performance Si/SiO₂-waveguide Bragg grating with 0.12-nm channel spacing.

Three-port WDM devices, in contrast to the two-port Bragg-grating device, can be constructed using ring resonators. A schematic of a resonator is shown in Fig. 11. When using a demultiplexer [Fig. 11(a)], light is coupled to the top waveguide, called the bus. The information is then transmitted or coupled to the bottom waveguide through the resonator. Light is coupled through the resonator only at specific resonance wavelengths given by

$$\frac{n_{\text{eff}} L}{\lambda_0} = m \quad (3)$$

where m is an integer number and L is equal to $2\pi R$, where R is the radius of the ring. All the other wavelengths are transmitted through the bus waveguide. When using a device as a multiplexer [Fig. 11(b)], light coupled to the bottom waveguide, with a frequency corresponding to one of the ring resonances, will couple to the top waveguide and will be transmitted through the bus along with the off-resonance signals propagating through the same bus. Si channel waveguides enable ring resonators to be extremely compact for high-bandwidth systems on-chip. Due to the high-index-contrast nature of the Si/SiO₂ platform, simulations and recent experimental results [11] show that ring resonators can be formed with radii as small as 0.9 μm with a round-trip bending loss of less than 0.5 dB.

By cascading several of these resonators, one can demultiplex or multiplex signals for WDM applications. A micrograph of a fabricated demultiplexing system in silicon is shown in Fig. 12. In [17], the authors show a high-performance WDM system based on a similar system.

Photonic-crystal waveguides have also been shown to have promising applications for passive devices on silicon. This is mainly due to their high-confinement nature, enabling ultra-compact structures. WDM filters, Mach-Zehnders, and couplers have been fabricated using photonic-crystal waveguides. Fig. 13 shows an example of a compact Mach-Zehnder device based on a photonic crystal. In [46] and [47], passive devices (as the ones described above for channel waveguides) of only a few micrometers in size were demonstrated using photonic-crystal waveguides.

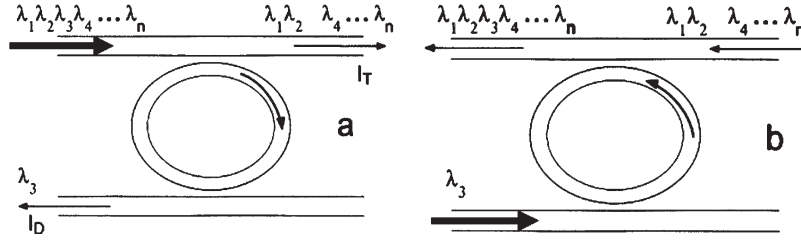


Fig. 11. Ring resonator used as a (a) demultiplexing or (b) multiplexing filter.

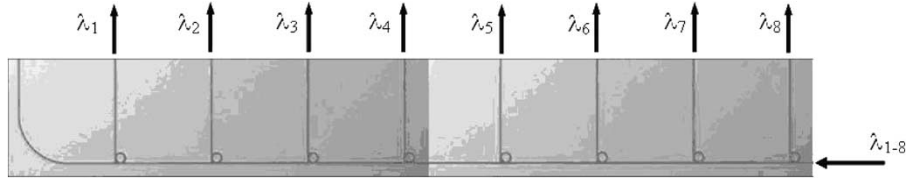


Fig. 12. Micrograph of a 1×8 multiplexer using multiple ring resonators.

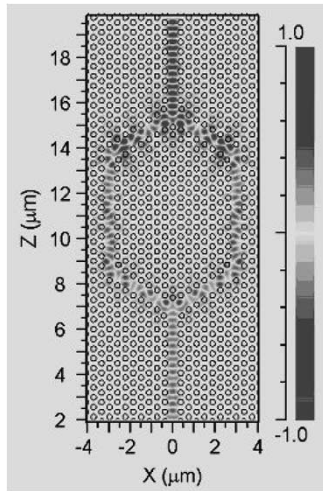


Fig. 13. FDTD simulation of a Mach-Zehnder using photonic-crystal waveguides.

III. ACTIVE SILICON DEVICES

Photonic structures that bend, split, couple, and filter light described in Section II-D have their flow of light predetermined by the structure design and cannot be modified once fabricated. In order to control the flow of light, modulators and switches need to be developed in silicon where a change in refractive index induces a change in the transmission properties of the device. Below, we describe possible geometrical configurations used as silicon modulators as well as the main physical mechanisms for modulating the refractive index of silicon.

A. Configurations for Modulation in Silicon

There are several device configurations that use an index change to directly modulate light intensity. These configurations rely on optical retardation. Under an index change, the wave experiences a phase shift (per unit-waveguide length) approximately given by

$$\Delta\beta = \Delta n \cdot k_o. \quad (4)$$

Assuming that the index change Δn is due to an applied electric field over a length L of the waveguide, the total phase shift is

$$\Delta\phi = \Delta\beta \cdot L = k_o \cdot L \cdot \Delta n = k_o \cdot L \cdot (\gamma E) \quad (5)$$

where L is the length over which the phase change $\Delta\phi$ occurs. γ is the change in effective index of the waveguide per applied field, which is also known as the linear electrooptic coefficient of the optical medium.

One of the most standard ways of converting a phase shift into intensity modulation is by using a Mach-Zehnder interferometer. In a modulator, if the relative phase difference of the waves traveling in the two arms varies by π , the intensity is modulated between 1 and 0. In order to create a π phase shift, from (5), the applied field needs to be

$$E = \frac{\lambda}{2\gamma L}. \quad (6)$$

Therefore, the longer the modulation length, the lower the field needed for modulation. In silicon, γ is extremely small: on the order of $10^{-3}/E$ (see the detailed description in Section III-B below). From (6), one can see that the required length for π phase shift for $\lambda = 1.55 \mu\text{m}$ is on the order of millimeters or longer. This required long length limits the Mach-Zehnder device to be used as a discrete device. The advantage of the Mach-Zehnder, however, is its low sensitivity to variations in temperature. In silicon, a change in index with temperature is approximately $2 \cdot 10^{-4}/\text{K}$ [15]. A change in the temperature environment of about 10° will change the phase shift by less than 1%.

An alternative approach that could enable high modulation in silicon using compact devices is the use of resonators. The transmission of a resonator is given approximately by

$$T = \frac{T_{\max}}{1 + \left(\frac{4n_L}{\pi \cdot \Delta\lambda}\right)^2 \sin^2\left(\frac{2\pi}{\lambda} n_L\right)} \quad (7)$$

where λ is the wavelength incident on the resonator and $\Delta\lambda$ is the width at half maximum of the transmission at resonance, determined by the quality of the resonator and its geometrical

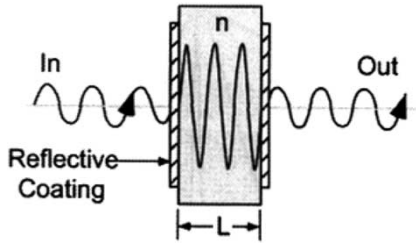


Fig. 14. Schematics of a Fabry-Pérot etalon.

configuration. Fig. 14 shows an example of a resonator, a Fabry-Pérot etalon consisting of two mirrors with reflectivity r spaced by a distance L on the order of the wavelength λ . For a resonator, at a resonance wavelength given by (3), light is trapped in the resonator. This ability of a resonator to circulate light within the cavity at the resonance wavelength can be used to increase the optical path length without increasing the physical-device length, unlike a Mach-Zehnder interferometer. In a high-quality resonator, the spectral width of the resonance is given by $\Delta\lambda = 2nL(1-r)/\pi\sqrt{r}$. After a typical photon lifetime in the resonator given by $\tau_{ph} = \lambda L/\Delta\lambda c$, light exits the device with transmissivity $T = T_{max}$. At all other wavelengths within the stopband, light destructively interferes in the cavity region and is not transmitted through the resonator (it is either reflected or directed to a different path, depending on the geometrical configuration of the modulator). Note that for waveguide resonators, typically micrometer in size with $\lambda/\Delta\lambda \sim 10^2-10^4$, the photon lifetime is typically short, on the order of a few picoseconds. This is important in order to guarantee the fast operation of the resonator as a modulator. In order to achieve modulation using resonators, the resonances of the device is tuned by modifying the index of refraction of the structure. Due to their strong-light-confinement nature, a small index-of-refraction change induces a strong tuning of the resonance. From (7), one can see that if the refractive index is changed by a small amount, the transmission can change significantly at or near resonance, resulting in a strong intensity modulation of the signal transmitted through the resonator. As an example, Fig. 15 shows the spectra of a resonator for two different effective indices n . One can see that if the probe wavelength corresponds to one of the resonances (dashed line), a strong modulation of the probe intensity occurs as a result of the spectral tuning (from 0.1 to 0.99 when the modulator is switched from the OFF state to the ON state).

Different types of resonators may be used as modulators. Resonators based on photonic crystals, microcavities, and rings have been demonstrated [17], [46], [47]. Fig. 16 shows three different types of resonators. In the photonic-crystal cavity [Fig. 16(a)], light is confined in a region surrounded by a totally reflecting photonic crystal. In the 1-D microcavity [Fig. 16(b)], light is confined in a waveguide region embedded between two distributed Bragg reflectors (DBR), defined by alternating periodic holes in the waveguide. In the ring resonator [Fig. 16(c)], light is confined in a ring-shaped waveguide that is only weakly coupled to an adjacent waveguide. The quality factor Q of the resonator $Q = \lambda/\Delta\lambda$ is determined by the geometry of the resonator. For the photonic-crystal cavity, it is determined by the size of the cavity and the reflectivity of the surrounding

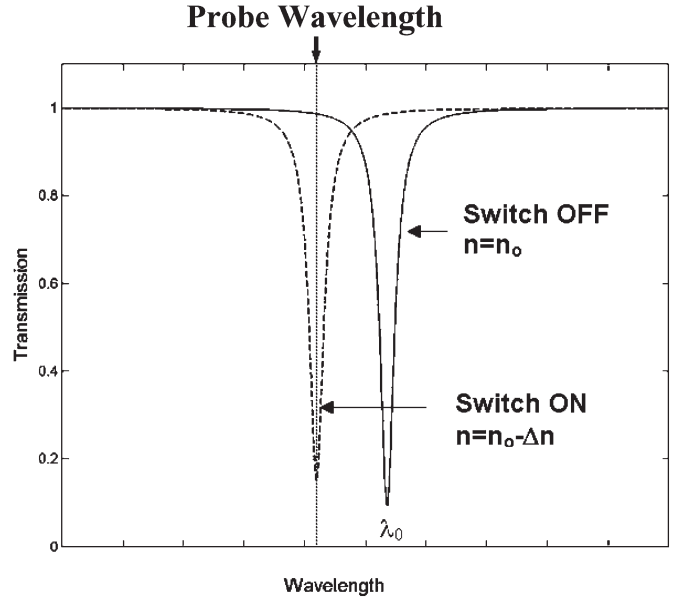


Fig. 15. Transmission spectra for two different indices in a resonator.

crystal. For the 1-D microcavity, it is determined by the size of the cavity and the reflectivity from the alternating periodic holes in the waveguide, and for the ring resonator, it is determined by the diameter of the ring and by the distance from the adjacent waveguide.

In [48], we use a ring resonator as a modulator for achieving high modulation in micrometer-size structures. For a ring resonator, we show that an index change as small as 10^{-3} is sufficient to tune the resonance by 1 nm and modulate the output intensity of the device by nearly 100%. This index change is achieved by carrier injection (the details of this effect are described below in Section III-B). The disadvantage of using resonators for modulation is the high temperature sensitivity of the device. For example, from (3), for $\lambda/\Delta\lambda \sim 10^3$, the silicon thermo-optic effect of $2 \cdot 10^{-4}/\text{degree}$ induces a modulation of approximately 5% for every degree change. In order to minimize the effect of the temperature variations on the index of refraction, recent studies have been investigating the use of strain in the waveguide structure between the silicon and the oxide cladding created by using a variety of oxidation methods for compensating for the effects of temperature variations on the index of refraction [49], [50].

B. Control of the Index of Refraction in Silicon

Modulation of the index of refraction of silicon can be done using the thermo-optic effect. The thermo-optic coefficient for silicon is typically three times greater than in classical thermo-optical materials and eight times greater than in silica-based materials. The effect, however, is rather slow and can only be used for up to 1-MHz modulation frequencies [51].

For high-speed modulation, electrooptic devices are required. The most common electrooptic effects used in compound semiconductors, however, are weak in silicon. Unstrained pure crystalline Si does not exhibit a linear electrooptic (Pockels) effect and the Franz-Keldysh effect (“electroabsorption”) and the Kerr effect (the second order

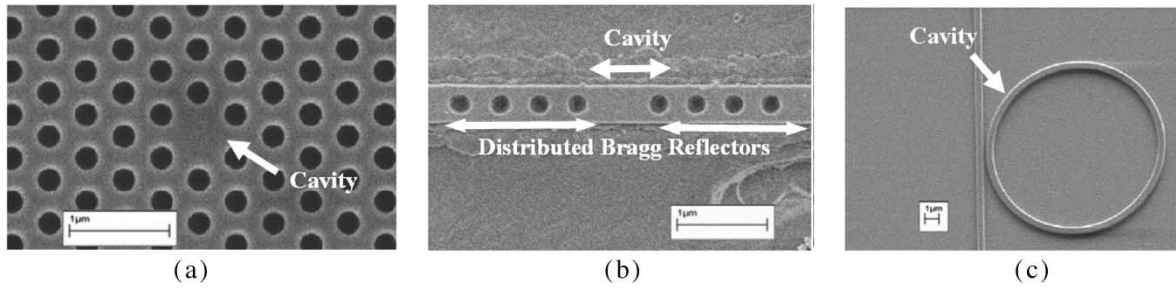


Fig. 16. SEM of three types of resonators: (a) A 2-D photonic-crystal cavity, (b) 1-D microcavity, and (c) a ring-resonator cavity.

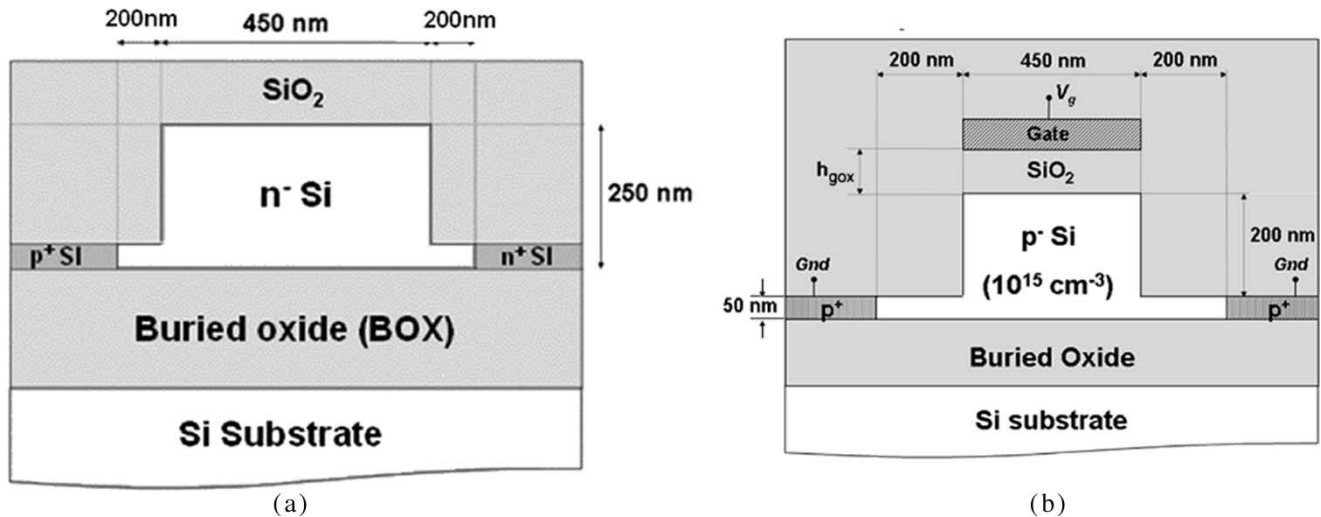


Fig. 17. (a) Schematic cross section of a ridge waveguide with an integrated lateral p-i-n diode for electrooptic modulation. (b) Schematic cross section of a ridge waveguide with an integrated MOS structure for electrooptic modulation.

electrooptic) have very low efficiency: a refractive-index variation of $\Delta n \sim 10^{-5}$ in the near infrared for the Franz-Keldysh effect and $\Delta n \sim 10^{-8}$ for the Kerr effect for an applied field of 10^5 V/cm. Therefore, high fields potentially close to the breakdown of Si are required to obtain a useful refractive index change.

The most effective mechanism for changing the refractive index in Si at a fast rate is the free-carrier plasma-dispersion effect [52], which also has the advantage of being polarization independent. The induced real refractive index and optical-absorption coefficient variations (Δn and $\Delta\alpha$, respectively) produced by free-carrier dispersion at a wavelength of $1.55 \mu\text{m}$ are given by [53]

$$\begin{aligned} \Delta n &= \Delta n_e + \Delta n_h \\ &= - [8.8 \times 10^{-22} \cdot \Delta N + 8.5 \times 10^{-18} \cdot (\Delta P)^{0.8}] \end{aligned} \quad (8)$$

$$\begin{aligned} \Delta\alpha &= \Delta\alpha_e + \Delta\alpha_h \\ &= 8.5 \times 10^{-18} \cdot \Delta N + 6.0 \times 10^{-18} \cdot \Delta P \end{aligned} \quad (9)$$

where Δn_e is the refractive-index change due to electron-concentration change, Δn_h is the refractive-index change due to hole-concentration change, ΔN (cm^{-3}) is the electron-concentration change, ΔP (cm^{-3}) is the hole-concentration change, $\Delta\alpha_e$ (cm^{-1}) is the absorption-coefficient variations due to ΔN , and $\Delta\alpha_h$ (cm^{-1}) is the absorption-coefficient variation due to ΔP . Thus, electrorefractive changes of

$\Delta n \sim 2 \times 10^{-3}$ at a wavelength of $1.55 \mu\text{m}$ can be produced with a depletion or injection of 10^{18} carriers/ cm^3 .

The free-carrier concentration can be varied in Si by injecting or generating carriers. In an electrooptic device, we can inject carriers by applying an electric field to the device in order to control the flow of light. In an all-optical device, we can generate carriers within the device using an optical pump source where one optical beam controls the flow of another.

In electro-optical devices, the carrier concentration can be varied by injection, accumulation, depletion, or inversion of carriers. Diodes (p-i-n) [54], [55] and MOSFETs [56], [57] may be employed for this purpose.

Fig. 17(a) shows a schematic cross section of a ridge waveguide with an integrated lateral p-i-n diode for electrooptic modulation [55]. It consists of a ridge waveguide with a p^+ region and an n^+ region defined in the slab at each side of the ridge. The waveguide is fabricated on an SOI wafer comprised of three layers, one single-crystal layer of silicon, a base silicon substrate, and a thin insulator (BOX) that acts as bottom cladding and, therefore, prevents light leakage to the substrate. The silicon layer (device layer) has an n-type background doping concentration of 10^{15} cm^{-3} , whereas a uniform doping concentration of $\sim 10^{19} \text{ cm}^{-3}$ for both p^+ and n^+ regions is considered. A top SiO_2 cladding layer covers the whole structure. Using configurations similar to the one shown in Fig. 17(b) in waveguides and interferometers, several devices have been demonstrated with speeds up to 20 MHz [55],

[57]–[68]. By embedding the ridge waveguide shown in Fig. 17(a) into a ring resonator with $Q = 40\,000$, Xu demonstrated in [20] a modulation depth of 15 dB with a modulation speed of 1.5 Gb/s. The high modulation speed was achieved using both forward and reverse bias for injecting and extracting carriers, respectively.

The use of an MOS diode should lead to higher speed operation [69] and very low dc-power consumption. Fig. 17(b) shows a schematic cross section of an MOS-waveguide configuration. The structure consists of a ridge SOI waveguide with highly doped regions (10^{19} cm^{-3}) defined in the slab at each side of the rib. The fact that the carriers are located only in a small region results in a small overlap between the optical mode and the nonequilibrium charge distribution in the waveguide, leading to a smaller effective-index variation in an MOS system than that in a p-i-n configuration. A small index change requires a very long structure, on the order of millimeters, in order to induce a significant modulation depth [see (5)]. Liu *et al.* have recently demonstrated a high-speed silicon optical modulator based on an MOS configuration [18]. The authors use an MOS configuration embedded in silicon waveguides in a Mach–Zehnder geometry and were able to demonstrate a modulation speed exceeding 10 Gb/s. Due to the weak dependence of the silicon refractive index on the free-carrier concentration, the devices in [18] have relatively long lengths: on the order of millimeters. MOS-based modulators can be miniaturized by embedding the above ridge waveguide into a resonator. Fig. 18 shows a schematic of a ring-resonator-based optical modulator using the MOS effect [18]. A gate electrode is placed close to the top of the ring resonator. Using the configuration in Fig. 17(b) with a gate oxide of $h_{\text{gox}} = 200\text{ nm}$, we estimate a change in index of approximately 6×10^{-5} under an applied voltage of 5 V. By embedding a structure in a resonant $20\text{-}\mu\text{m}$ -diameter device with $Q \sim 1000$ as the one in the figure, the changes in index induce 20% modulation depth for a gate voltage of 5 V [69]. The speed of the device is determined by its capacitance. Using the above geometrical parameters, the time constant $\tau_c = RC_T$ of the device is approximately $5 \times 10^{-15}\text{ s}/\mu\text{m}$. For a micrometer-size device, this translates into tens-of-gigahertz modulation frequencies. Note that the fundamental speed limitation, due to the photon lifetime in such a ring resonator (1 ps), is approximately 200 GHz.

In all-optical devices, the free carriers can be injected through one- [70] or two-photon absorption processes. In [48], the transmission of a silicon ring resonator was modulated by up to 94% in 500 ps. The pump source used was a picosecond pulse in the $1.55\text{ }\mu\text{m}$ light spectral range, with energy as low as 25 pJ. In this experiment, both the pump and probe beams with wavelengths corresponding to two adjacent resonances of the ring were coupled into the structure. The pump pulse generated a free-carrier concentration of $\Delta N = \Delta P = 1.6 \cdot 10^{17}\text{ cm}^{-3}$, by two-photon absorption, inducing a refractive-index change in the silicon core of $\Delta n_{\text{Si}} = -5.2 \cdot 10^{-4}$. This change in index induced a wavelength shift of the resonance of 0.36 nm, which is sufficient to modulate the probe pump by 94%. The modulation time of the device of 450 ps is determined by the free-carrier lifetime. This lifetime, which is much shorter than the one in bulk silicon, is not a fundamental limit on the speed;

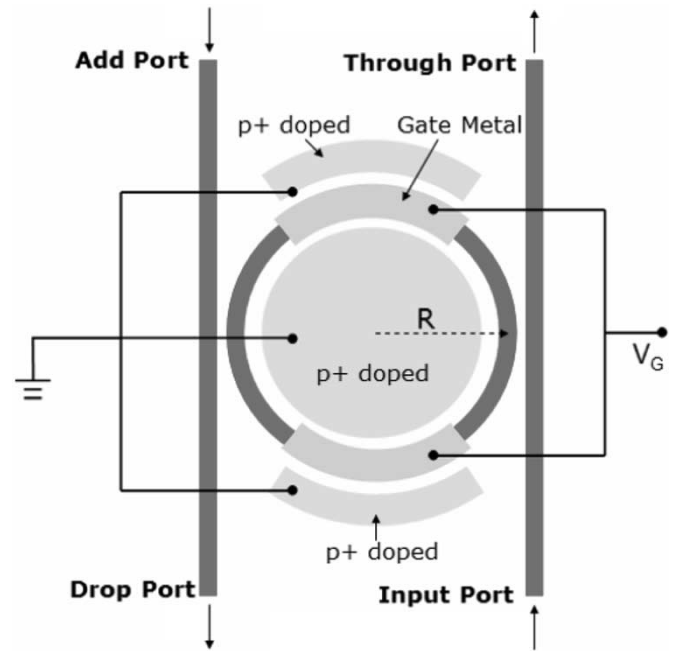


Fig. 18. Schematics of ring-resonator-based optical modulator using the MOS effect.

it is due primarily to fast recombination mechanisms on the unpassivated sidewalls of the structure. By manipulating the degree of surface passivation or by using ion implantation [71], the free-carrier lifetime could be further decreased.

IV. LIGHT SOURCE FOR SILICON PHOTONICS

Silicon, in contrast to conventional optical materials, as compound semiconductors, has a poor optical-emission cross section due to its indirect band gap. A silicon emitter is the missing piece for monolithic integration as it would enable all optical elements and drive electronics to be fabricated on a common substrate. Until a reliable and efficient silicon emitter can be produced, hybrid integration must be considered, using a nonsilicon-based light source from a fiber coupled to silicon waveguides. In this approach, the external light source acts as an “external photonic battery”: The signal from the source is distributed on the chip using waveguides, bends, and splitters. Since only a single external source is used, the cost of the Si photonic chip is not increased substantially due to the absence of monolithically grown silicon laser. In order to enable this hybrid approach, the problem of coupling large fibers to submicrometer-size waveguides must be addressed. In Section IV-A, we describe schemes for coupling external fibers to submicrometer-size waveguides.

While a silicon laser is still out of reach, work is being done worldwide on silicon light emitters. In Section IV-B, we describe schemes for achieving gain and lasing in silicon.

A. Tapers for Fiber–Waveguide Coupling

Typical fibers have mode sizes on the order of $\sim 10\text{ }\mu\text{m}$, contrasting with the much smaller mode size of waveguides (from a few micrometers down to submicrometer dimensions,

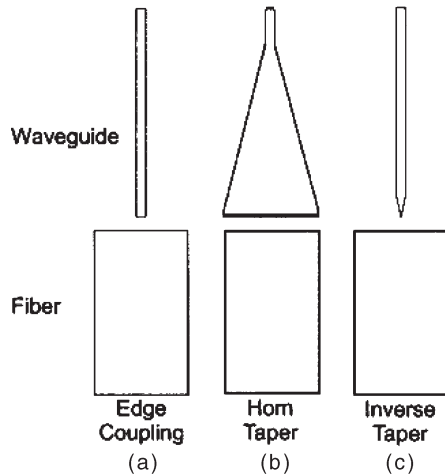


Fig. 19. Schemes for fiber-to-waveguide coupling. (a) Edge coupling. (b) Horn taper. (c) Inverse taper.

depending on the type of waveguide). Coupling between small-size waveguides and large-scale fibers has been a long-standing challenge in the field of integrated optics. This is due to both mode and index mismatch between the fiber and the waveguides, which induces coupling to radiation modes and back reflections. Ridge waveguides are typically larger, with cross-sectional dimensions of several micrometers, which make it easier to couple light in and out of them. Single-mode ridge waveguides with fiber-coupling losses as low as 0.17 dB per facet have been reported [43]. Channel waveguides, in contrast, typically have submicrometer cross-sectional dimensions and suffer from very high coupling losses.

The coupling efficiency between two waveguides with different propagation constants β_1 and β_2 and field amplitudes E_1 and E_2 is given by

$$\eta = \frac{4\beta_1\beta_2}{(\beta_1 + \beta_2)^2} \times \frac{[\int E_2(r, \phi) E_1^*(r, \phi) r dr d\phi]^2}{\int E_2(r, \phi) E_2^*(r, \phi) r dr d\phi \int E_1(r, \phi) E_1^*(r, \phi) r dr d\phi}. \quad (10)$$

Considering a fiber with a 10- μm mode-field diameter edge coupled to a channel silicon waveguide [Fig. 19(a)], using (10), the coupling efficiency is approximately 0.01. Clearly, simple edge coupling is not a viable scheme.

Tapers from the waveguide dimensions to the fiber dimensions, called “Horn tapers,” for improving coupling efficiency between optical fiber and waveguide modes [Fig. 19(b)], have been suggested [73]. However, in order to avoid excessive coupling to radiation modes in the taper, the required typical taper length must be on the order of millimeters. In addition, these tapers suffer from strong back reflections at the facet of the coupler.

Recently, there have been several demonstrations of good fiber-to-waveguide coupling using silicon structures with novel geometries. In [74], Manolatou and Haus suggest a taper based on high-refractive-index materials in order to decrease its length to about 5.5 μm . At the curved facet of the coupler, quarter wavelength plates are embedded, preventing back reflections,

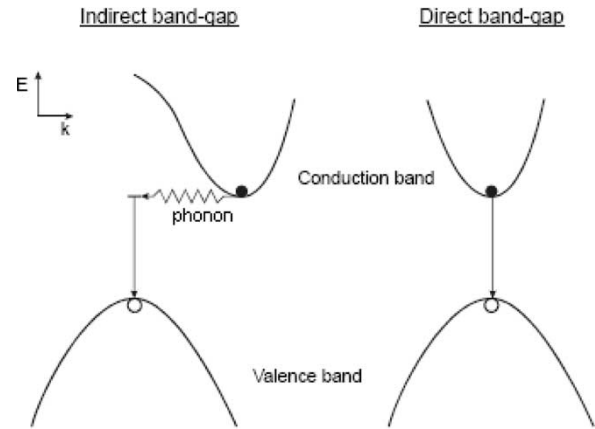


Fig. 20. Illustration of indirect and direct recombination in a semiconductor.

whereas layered structures with a graded index variation are introduced in the vertical direction. Almeida *et al.* recently proposed a micrometer-long nanotaper coupler that converts both the mode size and the effective index of the waveguide to that of the optical fiber [13]. The nanotaper consists of a highly confining waveguide tapered to a nanometer-sized tip at the facet, in contact with an optical fiber [Fig. 19(c)]. At the tip, due to its subwavelength dimensions, most of the field is expelled from the waveguide. However, the mode remained guided in the tip and is not lost to radiation due to the symmetry of the waveguide [32]. The net effect is a very large mode similar in effective index and profile to that of the fiber. By pointing the tip at the center of the fiber, the light from the fiber is completely drawn into the nanosized waveguide. Simulations based on the finite-difference time-domain (FDTD) and the beam-propagation method (BPM) show that the coupling losses using this device can be as low as 0.5 dB for a TE-like mode at $\lambda_0 = 1550$ nm with a tip width of 50 nm. A similar approach has been used in [14], where the authors use an inverse taper embedded in a 3 \times 3-micrometer high-index polymer channel waveguide. A relatively long taper of 200 μm length was used with a 60-nm tip width, in order to achieve a conversion loss of 1 dB. The authors measured a coupling efficiency of approximately 0.8 dB.

B. Lasing and Gain in Silicon

Achieving gain in silicon has been one of the most challenging goals in the area of silicon photonics. Luminescence in semiconductors is, in general, a result of electron–hole pair recombination. In the case of silicon, the energy band gap is indirect. Since the photon momentum is negligible, the recombination process requires the assistance of a phonon for momentum conservation (see Fig. 20). This reduces the probability of that process, resulting in a radiative lifetime around 100 ms above 20 K [75], [76].

At the same time, there are other nonradiative processes that compete with the radiative one as recombination through deep-energy-level traps that originate from impurities in the material and, at higher concentrations, Auger recombination (see Fig. 21). These competing mechanisms prevent population

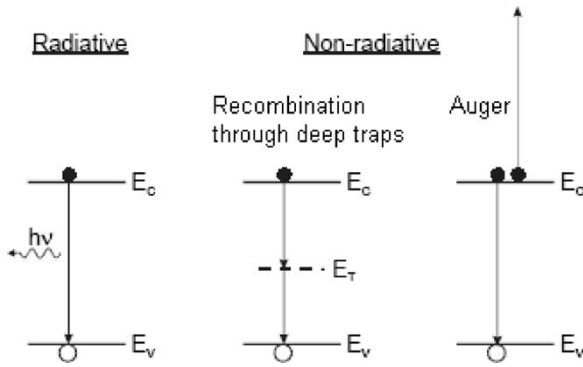


Fig. 21. Radiative and nonradiative recombination processes in semiconductors.

inversion at high pumping rates, which is critical for achieving gain. The luminescence efficiency is given by

$$\eta = \frac{\tau_{\text{nonrad}}}{\tau_{\text{nonrad}} + \tau_{\text{rad}}} \quad (11)$$

where τ_{rad} and τ_{nonrad} are the lifetimes of the radiative and nonradiative process. The efficiency of light emission in crystalline silicon is low, approximately 10^{-6} . This is because the nonradiative processes are relatively fast, sometimes with submicrosecond lifetimes. Despite the limitations of silicon as a light emitter, many different approaches have been employed to enable light emission in silicon [21]. Below, current efforts in increasing the luminescence efficiency of silicon and achieving gain is described. The efforts are directed towards: 1) decreasing the radiative lifetime relative to the nonradiative processes using quantum confinement (Section IV-B1) or Stimulated Raman emission (Section IV-B2); and 2) using the silicon as a host material for erbium—a light-emitting element (Section IV-B3).

1) *Quantum Confinement in Si-nc*: In order to increase the radiative recombination probability, carrier confinement can be employed. When a carrier is confined in real space, the k conservation rule may be partially relaxed due to Heisenberg's uncertainty relation $\Delta x \Delta k \geq 1$. Due to the quantum-confinement effect (Fig. 22), the band structure of Si-ncs is different from that of bulk silicon. Fig. 22 shows the schematics of the energy level in a small nanocrystal with typical dimension d_1 , and the energy levels in a large nanocrystal with typical dimension d_2 , $d_2 > d_1$. The energy gap of the large nanocrystal E_{g2} is similar to the one in bulk $E_{g,\text{bulk}}$, while the one of the small nanocrystal E_{g1} is much larger.

Carrier confinement can be achieved in silicon by producing Si-ncs in a silica matrix. In addition to the increase in radiative lifetime, the spatial confinement of the carriers prevents the recombination in deep traps, therefore increasing the nonradiative lifetime. The net effect is an increase of the luminescence efficiency by orders of magnitude.

Many different approaches have been proposed to form the nanocrystals [77]–[81]. The most widely used are based on the deposition of substoichiometric silica films, with a large excess of silicon, followed by high-temperature annealing. The annealing causes a phase separation between the two constituent phases, i.e., silicon and SiO_2 , with the formation of small

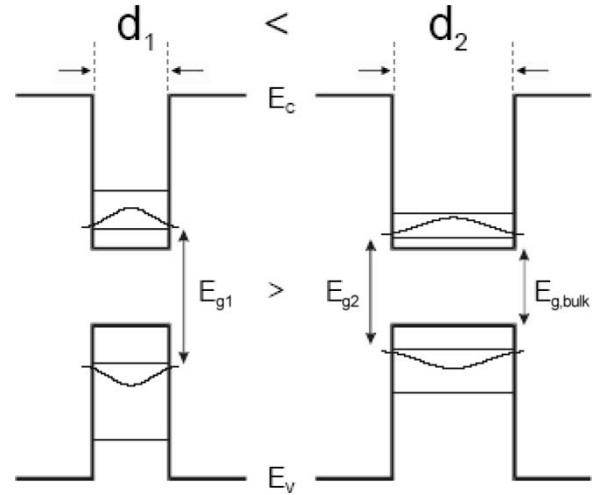


Fig. 22. Quantum confinement influence on the effective bandgap in small structures.

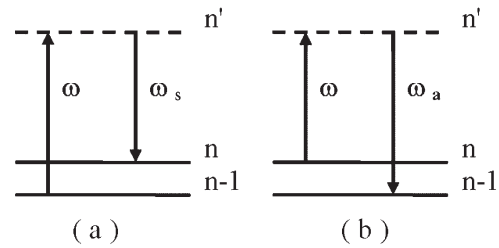


Fig. 23. Energy-level diagrams describing (a) Raman Stokes scattering and (b) Raman anti-Stokes scattering.

Si-nc. The size and density of the Si-nc can be controlled by the deposition and the annealing parameters.

Using Si-nc, Pavesi *et al.* demonstrated a gain of 12 cm^{-1} for a waveguide of 2-mm length at a wavelength of 760 nm [22]. Recently Atwater *et al.* reported a scheme for electrically pumping dense silicon nanocrystal arrays by a field-effect electroluminescence mechanism [82]. In this excitation process, electrons and holes are both injected from the same semiconductor channel across a tunneling barrier in a sequential programming process. Some challenges in using Si-nc remain and need to be addressed in order to achieve lasing in silicon using this approach. These are mainly 1) limitation on the pumping intensity at high excitation: With more than one electron–hole pair per crystallite, Auger recombination becomes efficient and leads to luminescence saturation; 2) Difficulty in integration with standard SOI waveguides: The emission wavelength is in the visible range, in the spectral range where the absorption in silicon is high.

2) *Raman Amplified Emission*: Raman scattering in crystals is caused by the interaction between the optical field and the lattice oscillations of the crystal. The scattering process can be understood with the energy diagram shown in Fig. 23 [83]. In Fig. 23(a), the crystal state is transferred from a lower oscillation state $n - 1$ to higher state n through a virtual level n' with the generation of a phonon. In this process, called Raman Stokes scattering, one pump photon at ω is absorbed and one Stokes photon at lower frequency ω_s is generated. The Raman anti-Stokes scattering process illustrated in Fig. 23(b), where a transition from the higher state to the lower state is

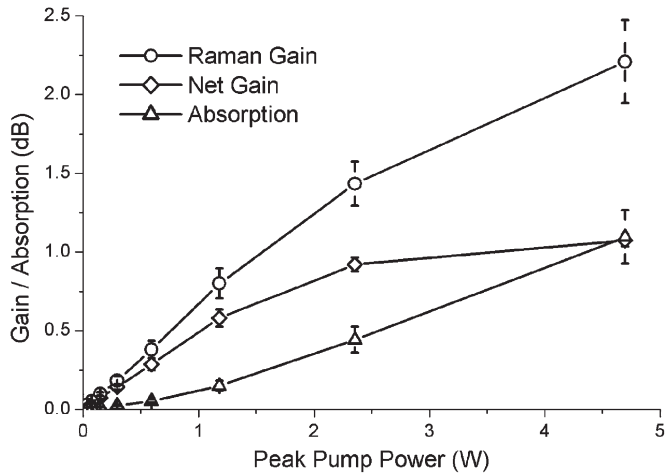


Fig. 24. Measured Raman gain (circles), net Raman gain (diamonds), and free-carrier absorption (triangles) versus the pump peak power.

accompanied by the emission of an anti-Stokes photon at higher frequency ω_a . This process has a much lesser probability of happening under thermal equilibrium due to the lower occupation rate of the higher state.

Spontaneous Raman scattering occurs when the pump photons are scattered by the thermal phonon. When both the pump field and the Stokes field are present, extra phonons can be generated coherently, which leads to stimulated Raman scattering.

Stimulated Raman scattering has been explored as a way to realize optical amplification [23]–[26] on silicon—taking advantage of the high Raman-scattering efficiency in crystalline silicon, which is orders of magnitude larger than the one in fibers. The Raman gain is inversely proportion to the cross-sectional area of the waveguide of propagation as [26]

$$G(\text{dB}) = 10 \log \int_0^L \left[\frac{g_s P_p(x)}{A} \right] dx \quad (12)$$

where P_p is the pump power, A is the mode area of the pump light, and g_s is the Raman-gain coefficient, and, therefore, can be enhanced using highly confined waveguides [25], [26].

The Raman gain in silicon waveguides is limited by the free-carrier absorption [24], [26]. The free carriers in the waveguides are generated by two-photon absorption; therefore, the carrier density and absorption rate are both proportional to the square of the pump power, while the Raman gain increases only linearly with pump power. This means that free-carrier absorption exceeds the Raman gain at high pump powers and causes net loss. This can be seen in Fig. 24 showing the measured Raman gain, the free-carrier absorption, and the net gain (Raman-gain absorption) versus the peak power of the pump pulse in a channel single-mode silicon waveguide. One can see that when the pump power is low, Raman gain increases linearly with the pump power, while the free-carrier absorption increases superlinearly with the pump power. The net Raman gain saturates at high pump powers (~ 2 W).

Despite the effect of the free-carrier absorption, strong net Raman gain can be observed in silicon waveguides using short pulses. This is because the free-carrier absorption is a much slower effect (typically nanoseconds) than stimulated

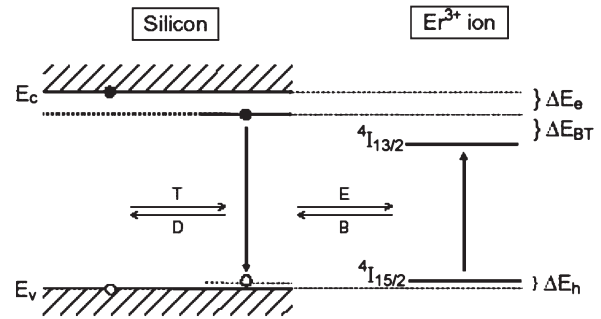


Fig. 25. Model of excitation and deexcitation of Er^{3+} in Si. Exciton trapping (T) and dissociation (D), Er^{3+} excitation (E) and energy backtransfer (B) are indicated by the horizontal arrows.

Raman scattering (femtoseconds). In [23]–[26], gain in the range of 2–11 dB has been reported in centimeter-sized silicon waveguides.

A Raman-based silicon laser was demonstrated in [27] using a compact waveguide cavity. The laser was pumped using a diode laser at $1.53 \mu\text{m}$, modulated using an acousto-optic modulator to produce pulses of 130 ns at 10 kHz. Note that although this silicon laser cannot be pumped electrically, this work represents a major step in silicon nanophotonics. A continuous-wave Raman silicon laser was demonstrated [84] by reducing the two-photon absorption effect using a reverse-biased p-i-n diode embedded in a silicon waveguide. The authors in [84] demonstrate stable single-mode laser output with a side-mode suppression of over 55 dB and a linewidth of less than 80 MHz.

3) *Er:Si*: The recent increase in the transmission capacity of optical fibers-based communication is related to the availability of all-optical amplifiers based on Er-doped fibers [85]. In these amplifiers, a silica optical fiber is doped with Er^{3+} ions, whose internal atomlike transitions at $1.54 \mu\text{m}$ is exploited to achieve light amplification. Several attempts have been made to reproduce a similar material system in silicon [86].

Si can be doped with optically active Er, using, for example, ion implantation [87]–[91] or molecular-beam-epitaxy techniques [92], [93]. Erbium in Si can be excited not only optically, but also electrically, in which electrical carriers transfer their recombination energy to the Er ions, which would allow for electrical pumping of an Er-doped Si planar waveguide amplifier. Erbium luminescence in crystalline silicon has been extensively studied in the past years [92], [94]–[99], [101]. Excitation spectroscopy has shown that Er photoluminescence in silicon, contrary to the luminescence of $\text{Er}:\text{SiO}_2$, is not caused by the resonant absorption of pump photons, but by excitation via optically generated electrons and holes. The excitation mechanism that has been proposed [96] to describe Er excitation in Si is shown in Fig. 25. In this model, electrons are trapped (T) at a deep level in the silicon bandgap, where they form a bound exciton. The deep level can be, for example, an impurity-induced level. Recombination of a bound e–h pair (exciton) can excite (E) the Er^{3+} 4f-shell in an Auger process. The erbium ion can then decay radiatively, resulting in the $1.54\text{-}\mu\text{m}$ luminescence.

Although relatively bright Er luminescence is commonly observed at low temperature ($T < 100$ K), in silicon, the luminescence intensity is found to decrease rapidly upon

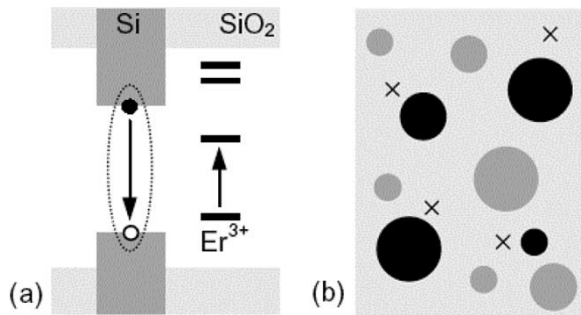


Fig. 26. (a) Er excitation model, showing the electronic-band structure of Si-nc-doped SiO₂ and the Er 4f energy levels. An optically generated exciton (dotted line) confined in the nanocrystal can recombine and excite Er³⁺. (b) Schematic representation of SiO₂ containing Er (crosses) and nanocrystals (circles) [99].

increasing the temperature to room temperature. The luminescence intensity can decrease as a result of the reverse process of exciton trapping (T): a dissociation (D) of the excitons in the bulk silicon. Since fewer excitons are formed, fewer are trapped at an Er³⁺ site and induce luminescence. The dissociation process requires thermal energy equal to the binding energy of the e-h pair ΔE_e , ΔE_h , and therefore, this process is increased with temperature. The decrease in luminescence with increase in temperature can also be a result of energy backtransfer (B) from excited erbium to a trapped carrier state in the silicon. The backtransfer process decreases the Er-excited-state lifetime, and with it, the Er luminescence efficiency. Due to the energy mismatch between excited Er and the localized exciton state indicated by ΔE_{BT} in Fig. 25, the backtransfer process also requires thermal energy. Consequently, as the temperature is increased, the Er lifetime is expected to decrease.

In order to minimize the backtransfer process, erbium can be implanted in silicon nanocrystals. The increase in bandgap energy decreases the backtransfer-efficiency process, since the energy mismatch ΔE_{BT} becomes larger and increases the erbium-luminescence efficiency. Fujii *et al.* reported that the presence of Si nanocrystals in Er-doped SiO₂ considerably enhances the effective Er absorption cross section [100]. In these systems, most of the erbium ions are located in the matrix. This increases the luminescence efficiency, since the SiO₂ materials system can support a much higher concentration of erbium ions ($10^{21}/\text{cm}^3$) than in silicon ($10^{18}/\text{cm}^3$). Thus, erbium doping of Si nanocrystals benefits from the advantages of both silicon (efficient excitation) and SiO₂ (high concentration).

Although the exact structural properties of the nanocrystals depend on the fabrication method employed, observations strongly suggest that energy is transferred from Si nanocrystals to the Er. A possible excitation model of the erbium ions in implanted silicon nanocrystals is shown in Fig. 26, which shows a schematic band diagram of SiO₂ containing a Si nanocrystal and Er³⁺. First, a photon is absorbed by the nanocrystal, which causes the generation of an exciton inside the nanocrystal. This exciton can recombine radiatively, emitting a photon with an energy that depends on the nanocrystal size. If an Er ion is present close to the nanocrystal, the exciton can recombine nonradiatively by bringing Er into one of its excited states.

MOS light-emitting devices operating at room temperature have been made in this system, demonstrating a quantum

efficiency greater than 1% [101]. The layer doped with Si-nc and Er³⁺ has a refractive index that is larger than that of SiO₂, which means that waveguides can be formed with a core containing Er coupled to Si-nc. Even though no net optical gain was measured [102], [103], an enhancement in the probe transmission at 1.55 μm was observed as the pump power was increased. A still-open question is to engineer the waveguide losses (due to the scattering off of the nanoparticles) in order to be able to measure net gain and not only signal enhancement in a pump-and-probe experiment. This seems only to be a problem of time and research efforts.

V. CONCLUSION

Research in the area of planar optics in silicon has been underway for more than a decade. However, it is only recently that active and passive photonic devices with high performance have been demonstrated. Novel mechanisms using advances in fabrication techniques have been developed for achieving ultracompact and low-loss silicon waveguides, fast electrooptical and all-optical modulators with very-low power, fiber-to-submicrometer-size-waveguides couplers, and preliminary demonstrations of light emission in silicon. These recent achievements, combined with the immediate need for silicon photonics for optical interconnects brings silicon photonics into focus as a viable future for commercial optoelectronics.

ACKNOWLEDGMENT

The author would like to thank the members of the Cornell Nanophotonics Group (<http://nanophotonics.ece.cornell.edu>) for their help in compiling this review and for their contributions to many of the works cited here, and L. C. Kimerling for his inspiration and numerous valuable discussions on this topic.

REFERENCES

- [1] D. A. B. Miller, "Optical interconnects to silicon," *IEEE J. Sel. Topics Quantum Electron.*, vol. 6, no. 6, pp. 1312–1317, Nov./Dec. 2000.
- [2] J. D. Meindl *et al.*, "Interconnect opportunities for gigascale integration," *IBM J. Res. Develop.*, vol. 46, no. 2/3, pp. 245–263, Mar./May 2002.
- [3] E. M. Mohammed *et al.*, "Optical I/O technology for digital VLSI," in *Proc. SPIE*, San Jose, CA, 2004, vol. 5358, pp. 60–70.
- [4] O. Kibar, D. A. Van Blerkom, C. Fan, and S. C. Esener, "Power minimization and technology comparisons for digital free-space optoelectronic interconnections," *J. Lightw. Technol.*, vol. 17, no. 4, pp. 546–555, Apr. 1999.
- [5] A. M. Pappu and A. B. Apse, "Analysis of intrachip electrical and optical fanout," *Appl. Opt.*, vol. 44, no. 30, p. 6361, Oct. 2005.
- [6] M. Salib, L. Liao, R. Jones, M. Morse, A. Liu, D. Samara-Rubio, D. Alduino, and M. Paniccia, "Silicon photonics," *Intel Technol. J.*, vol. 8, no. 2, p. 1442, 2004.
- [7] R. C. Johnson. (2002). "Intel reveals long-term goals for silicon photonics, sensors." *Electron. Eng. Times*. [Online]. Available: <http://www.eetimes.com/semi/news/OEG20020228S0033>
- [8] L. C. Kimerling, "Photons to the rescue: Microelectronics becomes microphotonics," *Electrochem. Soc. Interface*, vol. 9, no. 2, p. 28, 2000.
- [9] C. Gunn, "CMOs photonics-SOI learns a new trick," in *Proc. IEEE Silicon On Insulator (SOI) Conf.*, Honolulu, HI, 2005.
- [10] R. Soref and J. Lorenzo, "All-silicon active and passive guided-wave components for $\lambda = 1.3$ and $1.6 \mu\text{m}$," *IEEE J. Quantum Electron.*, vol. QE-22, no. 6, pp. 873–879, Jun. 1986.
- [11] Y. A. Vlasov and S. J. McNab, "Losses in single-mode silicon-on-insulator strip waveguides and bends," *Opt. Express*, vol. 12, no. 8, pp. 1622–1631, Apr. 19, 2004.

- [12] K. K. Lee, "Transmission and routing of optical signals in on-chip waveguides for silicon microphotonic," Ph.D. dissertation, Dept. Materials Science Eng., Mass. Inst. Technol., Cambridge, MA, 2001.
- [13] V. R. Almeida, R. R. Panepucci, and M. Lipson, "Nano-taper for compact mode conversion," *Opt. Lett.*, vol. 28, no. 15, pp. 1302–1304, Aug. 2003.
- [14] T. Shoji, T. Tsuchizawa, T. Watanabe, K. Yamada, and H. Morita, "Low loss mode size converter from 0.3 μm square Si wire waveguides to singlemode fibers," *Electron. Lett.*, vol. 38, no. 25, pp. 1669–1670, Dec. 2002.
- [15] P. D. Trinh, S. Yegnanarayanan, and B. Jalali, "Guided-wave optical circuits in silicon-on-insulator technology," in *Tech. Dig. Integrated Photonics Research Conf.*, Boston, MA, 1996, vol. 6, pp. 273–277.
- [16] T. E. Murphy, J. T. Hastings, and H. I. Smith, "Fabrication and characterization of narrow-band Bragg-reflection filters in silicon-on-insulator ridge waveguides," *J. Lightw. Technol.*, vol. 19, no. 12, pp. 1938–1942, Dec. 2001.
- [17] D. R. Lim, B. E. Little, K. K. Lee, M. Morse, H. H. Fujimoto, H. A. Haus, and L. C. Kimerling, "Micron-sized channel dropping filters using silicon waveguide devices," in *Proc. SPIE—Int. Soc. Optical Engineering*, Boston, MA, 1999, vol. 3847, pp. 65–71.
- [18] A. Liu, R. Jones, L. Liao, D. Samara-Rubio, D. Rubin, O. Cohen, R. Nicolaescu, and M. Paniccia, "A high-speed silicon optical modulation based on a metal-oxide-semiconductor capacitor," *Nature*, vol. 427, no. 6975, pp. 615–618, Feb. 2004.
- [19] L. Liao, D. Samara-Rubio, M. Morse, A. Liu, D. Hodge, D. Rubin, U. D. Keil, and T. Franck, "High speed silicon Mach-Zehnder," *Opt. Express*, vol. 13, no. 8, pp. 3129–3135, Apr. 2005.
- [20] Q. Xu, B. Shmidt, S. Pradhan, and M. Lipson, "Micrometer-scale silicon electro-optic modulator," *Nature*, no. 435, pp. 325–327, May 2005.
- [21] S. Ossicini, L. Pavesi, and F. Priolo, *Light Emitting Silicon for Microphotonic (Springer Tracts in Modern Physics)*. Berlin, Germany: Springer-Verlag, 2003.
- [22] L. Pavesi, L. Dal Negro, C. Mazzoleni, G. Franzò, and F. Priolo, "Optical gain in silicon nanocrystals," *Nature*, vol. 408, no. 6811, pp. 440–444, Nov. 2000.
- [23] R. Clap, D. Dimitropoulos, V. Raghunathan, Y. Han, and B. Jalali, "Observation of stimulated Raman amplification in silicon waveguides," *Opt. Express*, vol. 11, no. 5, pp. 1731–1739, Jul. 2003.
- [24] T. K. Liang and H. K. Tsang, "Role of free carriers from two-photon absorption in Raman amplification in silicon-on-insulator waveguides," *Appl. Phys. Lett.*, vol. 84, no. 15, pp. 2745–2747, Apr. 2004.
- [25] R. L. Espinola, J. I. Dadap, R. M. Osgood, Jr., S. J. McNab, and Y. A. Vlasov, "Raman amplification in ultrasmall silicon-on-insulator wire waveguides," *Opt. Express*, vol. 12, no. 16, pp. 3713–3718, Aug. 2004.
- [26] Q. Xu, V. R. Almeida, and M. Lipson, "Time-resolved study of Raman gain in highly confined silicon-on-insulator waveguides," *Opt. Express*, vol. 12, no. 19, pp. 4437–4442, Sep. 2004.
- [27] H. Rong, A. Liu, R. Jones, O. Cohen, D. Hak, R. Nicolaescu, A. Fang, and M. Paniccia, "An all-silicon Raman laser," *Nature*, vol. 7023, no. 433, pp. 292–294, Jan. 2005.
- [28] G. Masini, L. Colace, G. Assanto, H. C. Luan, and L. C. Kimerling, "Germanium on silicon pin photodiodes for the near infrared," *Electron. Lett.*, vol. 36, no. 25, pp. 2095–2096, Dec. 2000.
- [29] M. Jutzo and M. Berroth, "SiGe-based photodetectors for optical communication," in *Applications Properties of Silicon Germanium and SiGe:Carbon*, E. Kasper and K. Lyutovich, Eds. London, U.K.: INSPEC, 2000, pp. 342–348. ISBN 085296783 8.
- [30] J. Oh, S. K. Banerjee, and J. C. Campbell, "Metal-germanium-metal photodetectors on heteroepitaxial Ge-on-Si with amorphous Ge Schottky barrier enhancement layers," *IEEE Photon. Technol. Lett.*, vol. 16, no. 2, pp. 581–583, Feb. 2004.
- [31] K. K. Lee, D. R. Lim, H.-C. Luan, A. Agarwal, J. Foresi, and L. C. Kimerling, "Effect of size and roughness on light transmission in a Si/SiO₂ waveguide: Experiments and model," *Appl. Phys. Lett.*, vol. 77, no. 11, pp. 1617–1619, Sep. 2000.
- [32] J. Schmidtchen, A. Splett, B. Schüppert, and K. Petermann, "Low loss single mode optical waveguides with large cross-section in silicon-on-insulator," *Electron. Lett.*, vol. 27, no. 16, pp. 1486–1488, Aug. 1991.
- [33] R. A. Soref, J. Schmidtchen, and K. Petermann, "Large single-mode rib waveguides in GeSi-Si and Si-on-SiO₂," *IEEE J. Quantum Electron.*, vol. 27, no. 8, pp. 1971–1973, Aug. 1991.
- [34] J. D. Joannopoulos, R. D. Meade, and J. N. Winn, *Photonic Crystals: Molding the Flow of Light*. Princeton, NJ: Princeton Univ. Press, 1995.
- [35] S. Y. Lin, J. G. Fleming, D. L. Hetherington, B. K. Smith, R. Biswas, K. M. Ho, M. M. Sigalas, W. Zubrzycki, S. R. Kurtz, and J. Bur, "A three-dimensional photonic crystal operating at infrared wavelengths," *Nature*, vol. 394, pp. 251–253, Jul. 16, 1998.
- [36] M. Loncar, T. Doll, J. Vuckovic, and A. Scherer, "Design and fabrication of silicon photonic crystal optical waveguides," *J. Lightw. Technol.*, vol. 18, no. 10, pp. 1402–1411, Oct. 2000.
- [37] V. R. Almeida, Q. Xu, C. A. Barrios, and M. Lipson, "Guiding and confining light in void nanostructure," *Opt. Lett.*, vol. 29, no. 11, pp. 1209–1211, Jun. 2004.
- [38] Q. Xu, V. R. Almeida, and M. Lipson, "Experimental demonstration of guiding and confining light in nanometer-size low-refractive-index material," *Opt. Lett.*, vol. 29, no. 14, pp. 1626–1628, Jul. 2004.
- [39] C. Pollock and M. Lipson, *Integrated Photonics*. Boston, MA: Kluwer, 2003.
- [40] M. Heiblum and J. Harris, "Analysis of curved optical waveguides by conformal transformation," *IEEE J. Quantum Electron.*, vol. QE-11, no. 2, pp. 75–83, Feb. 1975.
- [41] C. Manolatu, S. G. Johnson, S. Fan, P. R. Villeneuve, H. A. Haus, and J. D. Joannopoulos, "High-density integrated optics," *J. Lightw. Technol.*, vol. 17, no. 9, pp. 1682–1692, Sep. 1999.
- [42] D. Nedeljkovic, M. Loncar, S. Kuchinsky, M. Mikhailov, A. Scherer, and T. P. Pearsall, "Waveguiding at 1550 nm using photonic crystal structures in silicon on insulator wafers," in *Optical Fiber Communication Conf. and Exhibit. Tech. Dig. Postconf. Edition*, Anaheim, CA, 2001, vol. 2, pp. TuC6-1–TuC6-3.
- [43] U. Fischer, T. Zinke, J.-R. Kropp, F. Arndt, and K. Peterman, "0.1 dB/cm waveguide losses in single-mode SOI rib waveguides," *IEEE Photon. Technol. Lett.*, vol. 8, no. 5, pp. 647–648, May 1996.
- [44] P. K. Tien, "Light waves in thin films and integrated optics," *Appl. Opt.*, vol. 10, no. 11, pp. 2395–2413, Nov. 1971.
- [45] K. K. Lee, D. R. Lim, and L. C. Kimerling, "Fabrication of ultralow-loss Si/SiO₂ waveguides by roughness reduction," *Opt. Lett.*, vol. 26, no. 23, pp. 1888–1890, Dec. 2001.
- [46] J. S. Foresi, P. R. Villeneuve, J. Ferrera, E. R. Thoen, G. Steinmeyer, S. Fan, J. D. Joannopoulos, L. C. Kimerling, H. I. Smith, and E. P. Ippen, "Photonic-bandgap microcavities in optical waveguides," *Nature*, vol. 390, no. 6656, pp. 143–145, Nov. 1997.
- [47] T. Yoshie *et al.*, "High quality two-dimensional photonic crystal slab cavities," *Appl. Phys. Lett.*, vol. 79, no. 26, pp. 4289–4291, Dec. 2001.
- [48] V. R. Almeida, C. A. Barrios, R. R. Panepucci, and M. Lipson, "All-optical control of light on a silicon chip," *Nature*, vol. 431, no. 7012, pp. 1081–1084, Oct. 2004.
- [49] S. M. Weiss, M. Molinari, and P. M. Fauchet, "Temperature stability for silicon-based photonic band-gap structures," *Appl. Phys. Lett.*, vol. 83, no. 10, pp. 1980–1982, Sep. 2003.
- [50] P. Cheben, D.-X. Xu, S. Janz, and A. Delâge, "Scaling down photonic waveguide devices on the SOI platform," in *Proc. SPIE—Int. Soc. Opt. Engineering*, San Diego, CA, 2003, vol. 5117, pp. 147–156.
- [51] C. Cocorullo, M. Iodice, I. Rendina, and P. M. Sarro, "Silicon thermo-optical micro-modulator with 700 kHz–3 dB bandwidth," *IEEE Photon. Technol. Lett.*, vol. 7, no. 4, pp. 363–365, Apr. 1995.
- [52] R. A. Soref and B. R. Bennett, "Electrooptical effects in silicon," *IEEE J. Quantum Electron.*, vol. QE-23, no. 1, pp. 123–129, Jan. 1987.
- [53] ———, "Kramers-Kronig analysis of E-O switching in silicon," *SPIE Integr. Opt. Circuit Eng.*, vol. 704, pp. 32–37, Sep. 1986.
- [54] C. Z. Zhao, E. K. Liu, G. Z. Li, Y. Gao, and C. S. Guo, "Zero-gap directional coupler switch integrated into a silicon-on-insulator for 1.3- μm -operation," *Opt. Lett.*, vol. 21, no. 20, p. 1664, Oct. 1996.
- [55] C. Angulo Barrios, V. R. Almeida, and M. Lipson, "Electrooptic modulation of silicon-on-insulator submicrometer-size waveguide devices," *J. Lightw. Technol.*, vol. 21, no. 10, pp. 2332–2339, Oct. 2003.
- [56] S. R. Giguere, L. Friedman, R. A. Soref, and J. P. Lorenzo, "Simulation studies of silicon electro-optic waveguide devices," *J. Appl. Phys.*, vol. 68, no. 10, pp. 4964–4970, Nov. 1990.
- [57] G. Cocorullo, M. Iodice, and I. Rendina, "All-silicon Fabry-Pérot modulator based on the thermo-optic effect," *Opt. Lett.*, vol. 19, no. 6, p. 420, Mar. 1994.
- [58] X. Xiao, J. C. Sturm, K. K. Goel, and P. V. Schwartz, "Fabry-Pérot optical intensity modulator at 1.3 μm —in silicon," *IEEE Photon. Technol. Lett.*, vol. 3, no. 3, pp. 230–231, Mar. 1991.
- [59] Y. L. Liu, E. K. Liu, S. L. Zhang, G. Z. Li, and J. S. Luo, "Silicon 1 \times 2 digital optical switch using plasma dispersion," *Electron. Lett.*, vol. 30, no. 2, pp. 130–131, Jan. 1994.
- [60] Y. Liu, E. Liu, G. Li, S. Zhang, J. Luo, F. Zhou, M. Cheng, B. Li, and H. Ge, "Novel silicon waveguide switch based on total internal reflection," *Appl. Phys. Lett.*, vol. 64, no. 16, pp. 2079–2080, Apr. 1994.
- [61] C. Z. Zhao, G. Z. Li, E. K. Liu, Y. Gao, and X. D. Liu, "Silicon on insulator Mach-Zehnder waveguide interferometers operating at 1.3 μm ," *Appl. Phys. Lett.*, vol. 67, no. 17, pp. 2448–2449, Oct. 1995.
- [62] M. Y. Liu and S. Chou, "High-modulation-depth and short-cavity-length

- silicon Fabry-Pérot modulator with two grating Bragg reflectors," *Appl. Phys. Lett.*, vol. 68, no. 2, pp. 170–172, Jan. 1995.
- [63] A. Cutolo, M. Iodice, A. Irace, P. Spirito, and L. Zeni, "An electrically controlled Bragg reflector integrated in a rib silicon on insulator waveguide," *Appl. Phys. Lett.*, vol. 71, no. 2, pp. 199–201, Jul. 1997.
- [64] A. Cutolo, M. Iodice, P. Spirito, and L. Zeni, "Silicon electro-optic modulator based on a three terminal device integrated in a low-loss single-mode SOI waveguide," *J. Lightw. Technol.*, vol. 15, no. 3, pp. 505–518, Mar. 1997.
- [65] C. Z. Zhao, A. H. Chen, E. K. Liu, and G. Z. Li, "Silicon-on-insulator asymmetric optical switch based on total internal reflection," *IEEE Photon. Technol. Lett.*, vol. 9, no. 8, pp. 1113–1115, Aug. 1997.
- [66] G. Coppola, A. Irace, M. Iodice, and A. Cutolo, "Simulation and analysis of a high-efficiency silicon optoelectronic modulator based on a Bragg mirror," *Opt. Eng.*, vol. 40, no. 6, pp. 1076–1081, 2001.
- [67] A. Sciuto, S. Libertino, A. Alessandria, S. Coffa, and G. Coppola, "Design, fabrication, and testing of an integrated Si-based light modulator," *J. Lightw. Technol.*, vol. 21, no. 1, pp. 228–235, Jan. 2003.
- [68] C. K. Tang and G. T. Reed, "Highly efficient optical phase modulator in SOI waveguides," *Electron. Lett.*, vol. 31, no. 6, pp. 451–452, Mar. 1995.
- [69] C. Barrios and M. Lipson, "Modeling and analysis of high-speed electro-optic modulation in high confinement silicon waveguides using metal-oxide-semiconductor configuration," *J. Appl. Phys.*, vol. 96, no. 11, pp. 6008–6015, Dec. 2004.
- [70] V. R. Almeida, C. A. Barrios, R. R. Panepucci, M. Lipson, M. A. Foster, D. G. Quzounov, and A. L. Gaeta, "All-optical switching on a silicon chip," *Opt. Lett.*, vol. 29, no. 24, pp. 2867–2869, Dec. 2004.
- [71] A. Chin, K. Y. Lee, B. C. Lin, and S. Horng, "Picosecond photoresponse of carriers in Si ion-implanted Si," *Appl. Phys. Lett.*, vol. 69, no. 5, pp. 653–655, Jul. 1996.
- [72] L. Kimerling, *Towards the First Silicon Laser*, vol. 93, L. Pavesi, S. Gaponenko, and L. Dal Negro, Eds. New York: Kluwer, 2003, p. 465.
- [73] I. Moerman, P. P. Van Daele, and P. M. Daneester, "A review on fabrication technologies for the monolithic integration of tapers with III-V semiconductor devices," *IEEE J. Sel. Topics Quantum Electron.*, vol. 3, no. 6, pp. 1308–1320, Dec. 1997.
- [74] C. Manolatu and H. Haus, "Compact mode-size converters for efficient coupling between fibers and integrated optical waveguides," in *Proc. Lasers and Electro-Optics Society (LEOS) Summer Topical Meetings*, 2001, vol. 31.
- [75] R. B. Hammond and R. N. Silver, "Temperature dependence of the exciton lifetime in high-purity silicon," *Appl. Phys. Lett.*, vol. 36, no. 1, pp. 68–71, Jan. 1980.
- [76] M. A. Tamor and J. P. Wolfe, "Drift and diffusion of free excitons in Si," *Phys. Rev. Lett.*, vol. 44, no. 25, pp. 1703–1706, Jun. 1980.
- [77] *Silicon Based Microphotonics: From Basics to Applications*, O. Bisi, S. U. Campisano, L. Pavesi, and F. Priolo, Eds. Amsterdam, The Netherlands: IOS, 1999.
- [78] M. H. Nayfeh, N. Barry, J. Therrien, O. Akcakir, E. Gratton, and G. Belomoin, "Stimulated blue emission in reconstituted films of ultrasmall silicon nanoparticles," *Appl. Phys. Lett.*, vol. 78, no. 8, pp. 1131–1133, Feb. 2001.
- [79] F. G. Grom, P. M. Fauchet, L. Tsybeskov, J. P. McCaffrey, H. J. Labbe, D. J. Lockwood, and B. E. White, "Microcrystalline and nanocrystalline semiconductors—2000," in *Proc. Materials Research Society Symp.*, Boston, MA, 2001, vol. 638, pp. F6.1.1–F6.1.6.
- [80] F. Iacona, G. Franzò, and C. Spinella, "Correlation between luminescence and structural properties of Si nanocrystals," *J. Appl. Phys.*, vol. 87, no. 3, pp. 1295–1303, Feb. 2000.
- [81] P. M. Fauchet, J. Ruan, H. Chen, L. Pavesi, L. Dal Negro, M. Cazzanelli, R. G. Elliman, N. Smith, M. Samoc, and B. Luther-Davies, "Optical gain in different silicon nanocrystal systems," *Opt. Mater.*, vol. 27, no. 5, pp. 745–749, Feb. 2005.
- [82] R. J. Walters, G. I. Bourianoff, and H. A. Atwater, "Field-effect electroluminescence in silicon nanocrystal," *Nat. Mater.*, vol. 4, no. 2, pp. 143–146, Feb. 2005.
- [83] R. Boyd, *Nonlinear Optics*, 2nd ed. San Diego, CA: Academic, 2003.
- [84] H. Rong, R. Jones, A. Liu, O. Cohen, D. Hak, A. Fang, and M. Paniccia, "A continuous-wave Raman silicon laser," *Nature*, vol. 433, no. 7027, pp. 725–728, Feb. 2005.
- [85] P. C. Becker, N. A. Olsson, and J. R. Simpson, *Erbium-Doped Fibre Amplifiers*. London, U.K.: Academic, 1999.
- [86] A. M. Agarwal, L. Liao, J. S. Foresi, M. R. Black, X. Duan, and L. C. Kimerling, "Low-loss polycrystalline silicon waveguides for silicon photonics," *J. Appl. Phys.*, vol. 80, no. 11, pp. 6120–6123, Dec. 1996.
- [87] A. Polman, G. N. van den Hoven, J. S. Custer, J. H. Shin, R. Serna, and P. F. A. Alkemade, "Erbium in crystal silicon: Optical activation, excitation, and concentration limits," *J. Appl. Phys.*, vol. 77, no. 3, pp. 1256–1262, Feb. 1995.
- [88] G. Franzò, S. Coffa, F. Priolo, and C. Spinella, "Mechanism and performance of forward and reverse bias electroluminescence at 1.54 μm from Er-doped Si diodes," *J. Appl. Phys.*, vol. 81, no. 6, pp. 2784–2793, Mar. 1997.
- [89] B. Zheng, J. Michel, F. Y. G. Ren, L. C. Kimerling, D. C. Jacobson, and J. M. Poate, "Room-temperature sharp line electroluminescence at $\lambda = 1.54 \mu\text{m}$ from an erbium-doped, silicon light-emitting diode," *Appl. Phys. Lett.*, vol. 64, no. 21, pp. 2842–2844, May 1994.
- [90] S. Coffa, G. Franzò, and F. Priolo, "High efficiency and fast modulation of Er-doped light emitting Si diodes," *Appl. Phys. Lett.*, vol. 69, no. 14, pp. 2077–2079, Sep. 1996.
- [91] J. Palm, F. Gan, B. Zheng, J. Michel, and L. C. Kimerling, "Electroluminescence of erbium-doped silicon," *Phys. Rev. B, Condens. Matter*, vol. 54, no. 24, pp. 17603–17615, Dec. 1996.
- [92] R. Serna, J. H. Shin, M. Lohmeier, E. Vlieg, A. Polman, and P. F. A. Alkemade, "Incorporation and optical activation of erbium in silicon using molecular beam epitaxy," *J. Appl. Phys.*, vol. 79, no. 5, pp. 2658–2662, Mar. 1996.
- [93] A. Reittinger, J. Stimmer, and G. Abstreiter, "Influence of the erbium and oxygen content on the electroluminescence of epitaxially grown erbium-doped silicon diodes," *Appl. Phys. Lett.*, vol. 70, no. 18, pp. 2431–2433, May 1997.
- [94] P. N. Favennec, H. l'Haridon, D. Moutonnet, M. Salvi, and M. Gauneau, "Optical activation of Er^{3+} implanted in silicon by oxygen impurities," *Jpn. J. Appl. Phys.*, vol. 29, no. 4, pp. L524–L526, Apr. 1990.
- [95] J. Michel, J. L. Benton, R. F. Ferrante, D. C. Jacobson, D. G. Eaglesham, E. A. Fitzgerald, Y.-H. Xie, J. M. Poate, and L. C. Kimerling, "Impurity enhancement of the 1.54- μm Er^{3+} luminescence in silicon," *J. Appl. Phys.*, vol. 70, no. 5, pp. 2672–2678, Sep. 1991.
- [96] F. Priolo, G. Franzò, S. Coffa, and A. Carnera, "Excitation and non-radiative deexcitation processes of Er^{3+} in crystalline Si," *Phys. Rev. B, Condens. Matter*, vol. 57, no. 8, pp. 4443–4455, Feb. 1998.
- [97] S. Coffa, G. Franzò, F. Priolo, A. Polman, and R. Serna, "Temperature dependence and quenching processes of the intra-4f luminescence of Er in crystalline Si," *Phys. Rev. B, Condens. Matter*, vol. 49, no. 23, pp. 16313–16320, Jun. 1994.
- [98] T. Gregorkiewicz, D. T. X. Thao, J. M. Langer, H. H. P. T. Bekman, M. S. Bresler, J. Michel, and L. C. Kimerling, "Energy transfer between shallow centers and rare-earth ion cores: Er^{3+} ion in silicon," *Phys. Rev. B, Condens. Matter*, vol. 61, no. 8, pp. 5369–5375, Feb. 2000.
- [99] P. G. Kik, "Energy transfer in erbium doped optical waveguides based on silicon," Ph.D. dissertation, Nanophysics Dept., FOM-Inst. Atomic and Molecular Phys., Amsterdam, The Netherlands, 2000.
- [100] M. Fujii, M. Yoshida, Y. Kanzawa, S. Hayashi, and K. Yamamoto, "1.54 μm photoluminescence of Er^{3+} doped into SiO_2 films containing Si nanocrystals: Evidence for energy transfer from Si nanocrystals to Er^{3+} ," *Appl. Phys. Lett.*, vol. 71, no. 9, pp. 1198–1200, Sep. 1997.
- [101] F. Iacona, D. Pacifici, A. Irrera, M. Miritello, G. Franzò, F. Priolo, D. Sanfilippo, G. Di Stefano, and P. G. Fallica, "Electroluminescence at 1.54 μm in Er-doped Si nanocluster-based devices," *Appl. Phys. Lett.*, vol. 81, no. 17, pp. 3242–3244, Oct. 2002.
- [102] X. Zhao, S. Komuro, H. Isshiki, Y. Aoyagi, and T. Sugano, "Fabrication and stimulated emission of Er-doped nanocrystalline Si waveguides formed on Si substrates by laser ablation," *Appl. Phys. Lett.*, vol. 74, no. 1, pp. 120–122, Jan. 1999.
- [103] H.-S. Han, S.-Y. Seo, and J. H. Shin, "Optical gain at 1.54 μm in erbium-doped silicon nanocluster sensitized waveguide," *Appl. Phys. Lett.*, vol. 79, no. 27, pp. 4568–4570, Dec. 2001.



Michal Lipson (M'02) received the B.S., M.S., and Ph.D. degrees in physics from the Technion—Israel Institute of Technology, Haifa, Israel.

In December 1998, she joined the Department of Material Science and Engineering, Massachusetts Institute of Technology (MIT), Cambridge, as a Postdoctoral Associate. She joined the School of Electrical and Computer Engineering, Cornell University, Ithaca, NY, in 2001 as an Assistant Professor. Her research at Cornell University involves novel on-chip nanophotonics devices. She is the author of over

100 papers in major research journals and conferences in physics and optics.

Dr. Lipson is the Chair for the Integrated Optics Technical Group, OSA, and is the Topical Editor of *Optics Letters*. She was the recipient of the National Science Foundation (NSF) Career award in 2004.